By Architects. For Architects.
By Engineers. For Engineers.

Architecture and Engineering

Volume 3   Issue 4

CONTENTS

BIOMIMICRY ARCHITECTURE, FROM THE INSPIRATION BY NATURE TO THE INNOVATION OF THE SAHARAN ARCHITECTURE

Yassine Mohammed Benyoucef, Andrey Razin

Peoples' Friendship University of Russia
Miklukho-Maklaya Street, 6, Moscow, Russia

b.yassine@mail.ru

Abstract

Biomimicry is an old approach, but in the scientific conceptualization is new, as an approach of innovation based on the emulation of Nature, in recent years, this approach brings many potential theories and innovations in the architecture field. Indeed, these innovations have changed our view towards other Natural organisms also to the design processes in architecture, now the use of the biomimicry approach allows the application of a great sustainable development. The Sahara area is heading towards a sustainable policy with the desire to develop this rich context in terms of architecture. This article discuss the using of biomimetic strategy in the sustainable development of Saharan architecture.

The aim of the article is to present a synthesis of biomimicry approach and propose the biomimicry as a solution for the development of Saharan architecture which can use this approach as a sustainable and innovation strategy. The biomimicry is the solution for effective strategies of development and can have a great potential point to meet the current challenges of designing efficient for forms or structures, energy efficiency, and climate issues. Moreover, the Sahara can be a favorable soil for great changes, the use of this approach is the key for the most optimal strategies and sustainable development of the Saharan architecture. .

Keywords

Biomimicry, Sahara, architecture, nature, innovation, technology.

Introduction

Biomimicry, defined as a new engineering inspired by Nature, for innovation in different fields, design, transportation, architecture. As an interdisciplinary field, architecture is influenced by many aspects of the natural and technology and social sciences. Among these influences, the inspiration of biology is currently dominant. The framework of bio-inspired design has evolved and turned into different innovative approaches, largely due to the development of computing and its use in architecture (Chayaamor-Heil, Guéna, 2018).

After the emergence of this approach that makes the relationship between biology and architecture and also technology in architecture, Biomimicry defines as an innovative constructive approach to designs or a process of innovation inspired by nature.

In the worldwide, the United States is a leader in Biomimicry, and the latter is becoming increasingly important with New Research and Projects. Germany is the European leader with more than 80 research groups, the universities of Stuttgart, Freiburg and Tübingen, Germany, have joined forces to create a center of excellence dedicated to the bio-inspired design of building structures (Raskin, 2017).

Biomimicry design is not only adapting the design from the nature but also considering how to use nature's effective functions such as heating and cooling system (Rajshekhar Rao, 2014).

The historical part allowed becoming aware that nature has always been a reference for every population. Here are some historical landmarks (Figure 1) that spotted this evolutionary approach:

| 1485 | 1905 | 1949 | 1962 | 2009 | 2013 |
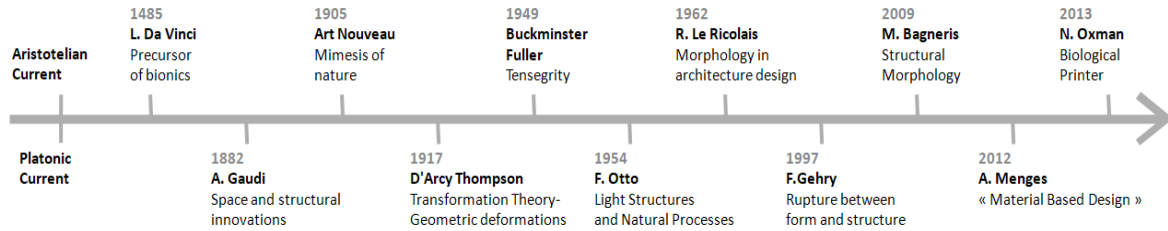
Figure 1. Architecture and the evolution of naturalistic thought. Source: Adeline STALS.

The term Biomimicry appears since 1980 by the biologist and environmentalist Janine Benyus, the author of the book "Biomimicry: Innovation Inspired by Nature" Benyus suggests looking at nature as a **Model, Measure, Mentor.**

In the scientific conceptualization, J. M. Benyus (1997) proposed as a definition of Biomimicry: "Innovation approach, which involves the transfer and adaptation of the principles and strategies developed by living organisms and ecosystems, to produce goods and services in a sustainable manner, and to make human societies compatible with the biosphere ... "

Architecture follows nature

Nature always offering immense inspirations and ideas to designers for creating architecture. Nature is demonstrably sustainable, her challenges have been resolved over eons to enduring solutions with maximal performance using minimal resources (Nori Oxman, 2010).

We always need to go back to nature, and architecture considered nature as a source of inspiration. As we have seen, the Biomimicry is that science which makes the intersection between biology and other disciplines, and this approach always asks the following questions:

How does nature help us to innovate? And how we can develop the architecture filed or other science from the concept of the bio-inspiration?

According to Frei Otto, the biology has become indispensable for architecture but architecture has also become indispensable for biology. In architecture, the bio-inspiration is perceived as a better method to answer the stakes of the design of forms and efficient structures, of energy efficiency and also at the level on the urban scale (Raskin, 2017), and the materials are also made by nature (Benyus, 2011). The goal of biomimetic architecture is not only to shape and measure space but also to develop synergistic relationships between the building and its environment (Chayaamor-Heil, 2018).

Figure 2. Elytra Filament Pavilion for Victoria & Albert Museum in London. With the using of robotics technologies (https://www.designboom.com/architecture/elytra-filament-pavilion-robotic-fabrication-victoria-and-albert-museum-london-05-18-2016/).

The biomimetic approach

The Biomimetic Concept:

Biomimicry = Science X + Biology.

Science X = Engineering, Architecture, Agricultural, Design, Mechanics, Industrial, Robotics, Management etc. Biomimicry or bio-inspiration approaches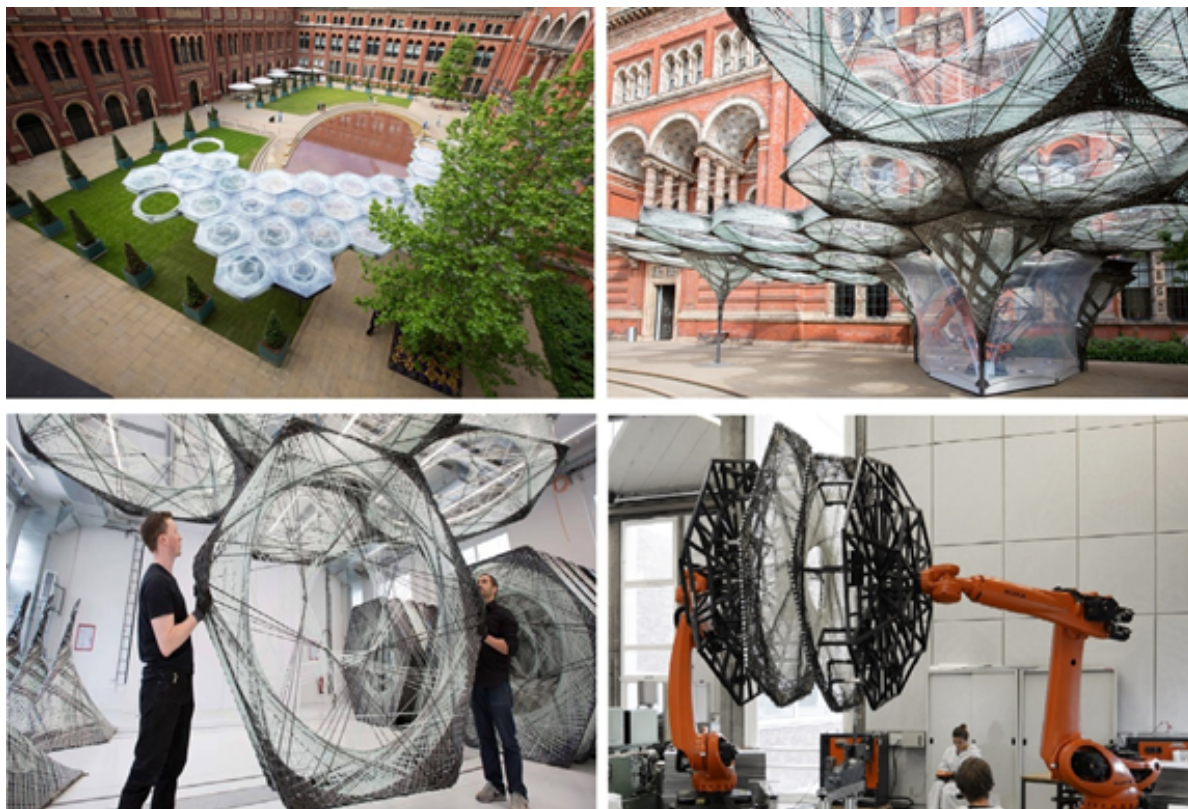 are very diverse, we consider the biomimetic design process as a whole, from the initial idea to the final product, and two approaches have been identified (Chayaamor-Heil, Guéna, 2018).

The first part concerns the design problem and then examines the ways in which organisms or ecosystems found in nature solve this problem. The second approach is to identify a particular characteristic, behavior, or function in an organism or ecosystem, and then look for the design problem that could be addressed.

We can distinguish in the process three main sections (Chayaamor-Heil, Guéna, 2018):

1- The search for the biological basis.

2- The abstraction of the results.

3- Implementation in design and technology.

Biomimicry, which is one of the most important science, by functionalities and by systems, which we can find and observe in Nature to develop sustainable innovations from an ecological point of view. This concept of innovation has a lot of advantages and a practical point of view.

The three levels of biomimicry in architecture:

Many of the architects developed architectural projects and constructions at the crossroads between biology and computer science and architecture. This development is at two levels the theoretical level and the practical level,

For example, Frank Gerry's works, characterized by wild, rupture entre la form and function, sweeping curves, and other projects which they use the advances

Table 1. Three possible levels of imitation and their description.

The three levels of imitation	The approaches	Description
The level of the organism	Formal	At the organism level corresponds to a biomimetic shape or surface. It is a question of the inspiration from forms found in nature. The organisms in nature and their morphology are perfectly adapted to the environment in which they live.
		The projects
		Elytra Filament Pavilion (Figure 2) in Victoria & Albert Museum in London which is an impressive example which explains the intersection between architecture and biology and the robotics. Its individual modules were defined by an algorithm and then produced with the help of an industrial robot, realized by a team from the University of Stuttgart. The second project is the design of the Art-Science Museum was inspired by the lotus flower (Figure3). The particular arrangement of the petals that make up the building allows rainwater to be collected for recycling and lets in natural light in several decreasing directions.
The level of behavior	Functional	At the behavior level corresponds to the function. It's about observing how nature performs a function.
		The projects
		One of the examples of the biomimetic technical solutions, the work of architect Mick Pearce illustrates the level of behaviour of Biomimicry in the Eastgate Building in Harare, Zimbabwe. It is partly based on ventilation and temperature control techniques observed in termite mounds in order to create a stable thermal environment inside the building (Figure 4). This passive ventilation system considerably reduces energy consumption.
The Level of ecosystem	Eco-systemic	The ecosystem-level corresponds to imitate ecosystems found in nature and considered as a means of increasing the sustainability of an architectural project. It is about understanding how relationships between species and their environment produce an ecosystem and It is characterized by his organization, hierarchy, interdependence, Dynamic, Adapted. The world's ecosystems are very complex and those characteristics what keep the planet as a whole in balance.
		The projects
		Among the examples, the Sahara Forest Project in Tunisia is a new environmental solution designed to utilize what we have enough of to produce what we need more of using deserts, saltwater, sunlight and CO_2 to produce food, water and clean energy.
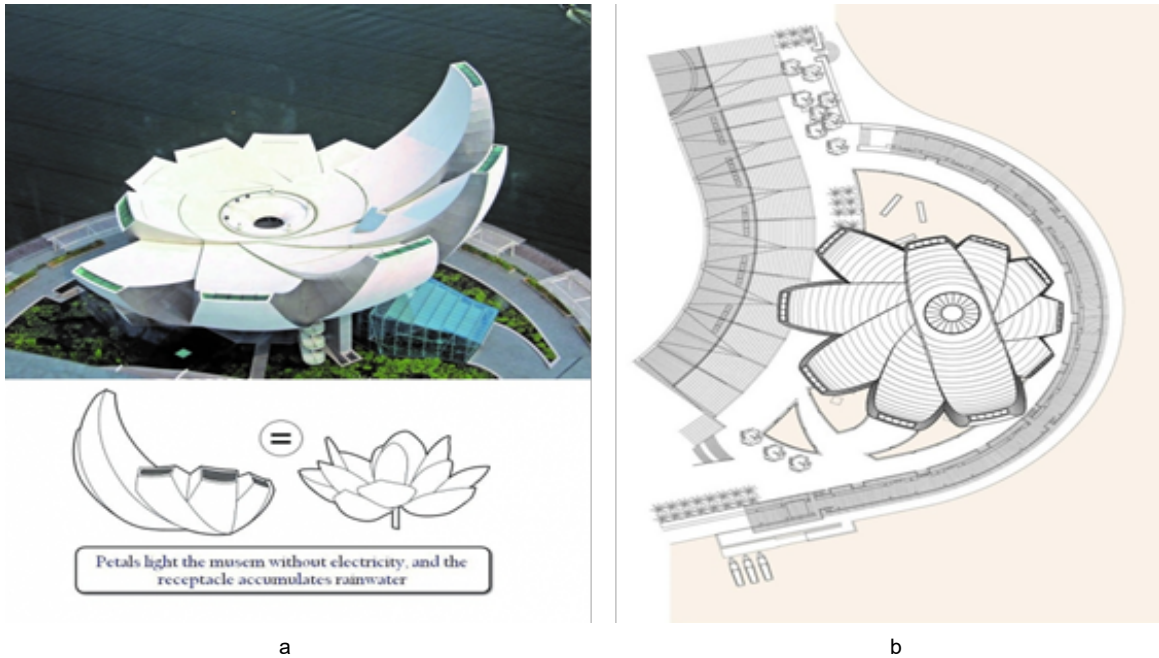
Figure 3. a – The Art-Science Museum, designed by architect Moshe Safdie, inspired by the lotus flower. b – Roof plan of the museum. Singapore (https://journals.openedition.org/craup/309, https://www.area-arch.it/en/artscience-museum/).
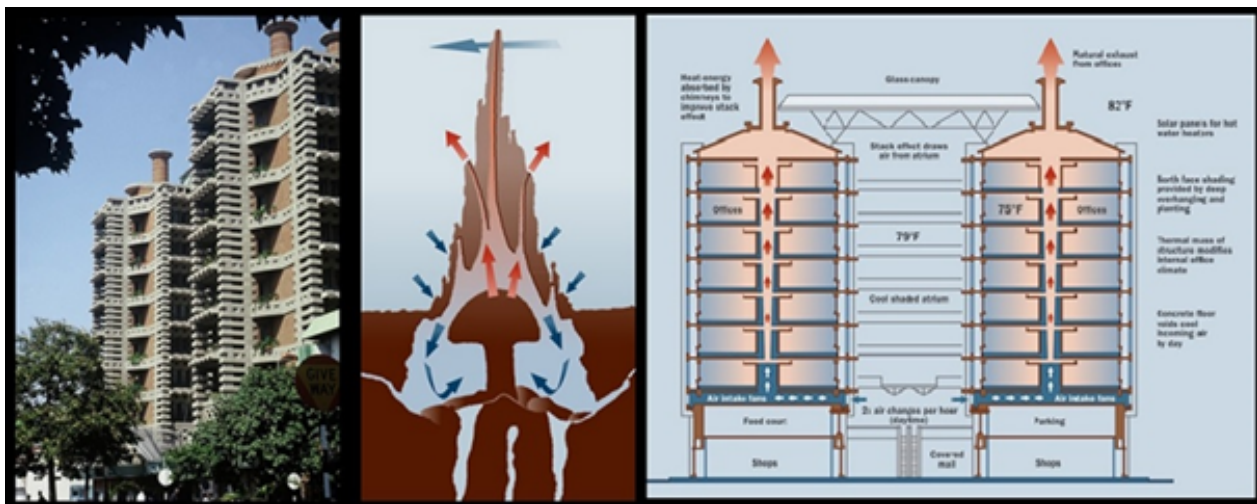
Figure 4. The termite mound ventilation system and the application of the termite mound operation to the natural ventilation of the Eastgate Building (https://journals.openedition.org/craup/309).

Figure 5. Physarum polycephalum in his Natural habitat (http://sweetrandomscience.blogspot.ru/2014/01/le-metro-de-tokyo-et-les-routes-des.html).

in 3D printing technology are often lauded as examples of biomimetic architecture.

The biomimetic design processes in architecture reveal three possible levels of imitation: the level of the organism, the behavior or the ecosystem (URBEO, 2010).

A biomimetic algorithm. A gooey Mold inspires the design of transport networks

When a team of Japanese and Hungarian researchers discovers that a kind of gooey Mold called Physarum Polycephal (Figure 5) is able to find its way in a labyrinth (Madjer, 2014). This Mold seems to be intelligent and able to explore its environment to find the shortest paths to food, and this was the first biological basis which was the base for the project.

Here is how the researchers proceeded to reproduce, at the scale of Physarum, the problematic of the network of Tokyo, which connects the capital to the 36 neighboring cities: they had 37 food points, corresponding to the 36 cities and Tokyo, in a box Petri, trying to respect the geography of the region. Then, they implanted Physarum at the point corresponding to Tokyo (the yellow dot in
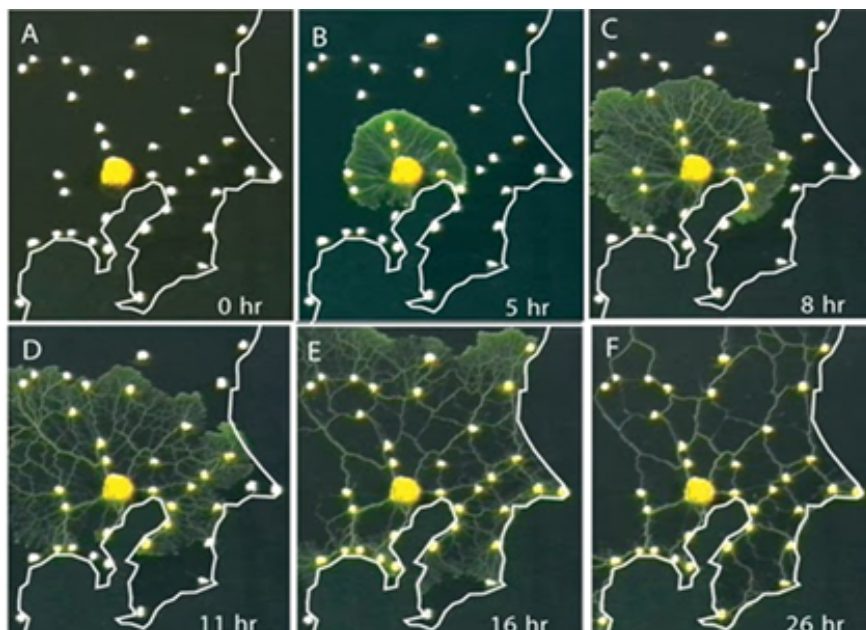
Figure 6. The evolution of the Physarum network in a Petri dish representing the Tokyo region (http://
sweetrandomscience.blogspot.ru/2014/01/le-metro-de-tokyo-et-les-routes-des.html).

Figure 6 below) and observed how the Mold was growing (Chayaamor-Heil, Guéna, 2018).

On the basis of these observations, an algorithm is constructed that mimics the behavior of the Physarum Polycephal: the Physarum Solver. This algorithm is able to find an optimal path in a network and be more efficient. This amazing algorithm can, for example, solve problems of optimization of a transport network. And give us the optimal answer of how we can connect cities in a minimum of lines with maximum efficiency and performance.

The examples of bio-inspiration are numerous, this review proposes to review the project's applications of this approach and identify the characteristics and methods of innovations and her development.

The examples presented show that the architectural biomimetic approach is an interdisciplinary approach combining biology and architecture and can give us the most optimal solutions to any architectural problems or for the new project's designs.

We can also mention the project designed by Achim Menges. This architect reproduces the biological principles of the pine cone (Figure 7). Indeed, it has developed a particular hygroscopic behavior, according to the moisture content of the air, it opens or retracts.

Figure 7. The biological principles of the pine cone, HygroSkin Meteorosensitive Pavilion (http://www.anabf.org/pierredangle/magazine/
europe-et-international/architecture-bio-inspiree-vers-la-conception-dhabitats-r-g-n-ratifs)

Figure 8. HygroSkin Meteorological Hall, Achim Menges in collaboration with Olivier David Krieg and Steffen Reichert, University of Stuttgart
(http://www.anabf.org/pierredangle/magazine/europe-et-international/architecture-bio-inspiree-vers-la-conception-dhabitats-r-g-n-ratifs)

Figure 9. Interface or the framework for FIT approach, Fully Integrated Thinking™
(http://www.hok.com/thought-leadership/fully-integrated-thinking/).

This phenomenon and the anisotropy of wood, in general, to understand and thus apply to architectural elements and represent the behavior level corresponds to the function.

In 2012, he designed HydroSkin, Meteorosensitive Pavilion (Figure 8), typically conceived as a technical function which reacts to climatic variations. Nature has evolved a variety of dynamic systems interacting with climatic conditions like the pine cone. For Achim Menges he starts from the material to generate the form, it is the characteristic of the trend of the material-based design.

At the intersection between biology and architecture, computer sciences

The world of biology is a great source of inspiration for the work of architects. For example, the architect Frei Otto's interest in biology is explained by his design of Lightweight constructions. While the Japanese Metabolists were interested in the biological processes of growth because they could apply to urban structures, Frei Otto was passionate about the optimization of natural structural forms. Frei Otto's interest in biology is explained by his recognition that the processes of evolution of natural forms are due to the biological laws of selection that generate lightweight constructions (Stals, 2013).

The mathematical, biological, physical developments and also computer advances of recent decades and the appearance of bionics, refocus attention on natural morphologies. Whatever the computer and mathematical methods at the heart of these various software programs, the increasing amount of data to be processed brings the actors of this form of bioinformatics to develop them more and more [Georgia Barlovatz-Meimon, Sylvain Sené, 2018].

Computer science, considered as a science or technology, has a growing role in the development of research in biology (Barlovatz-Meimon, Sené, 2018), and in architecture and other sciences. The advent of

computing has facilitated the design and modeling of complex shapes. The 2000s are marked by the emergence of "genetic algorithms". Genetic algorithms are a type of optimization algorithm, meaning they are used to find the maximum or minimum of a function (Carr, 2014), that is to say, mathematical formulas based on techniques derived from genetics and natural evolution to generate forms and develop new optimization models. In architecture, this means formalizing the design process according to a set of specific procedures and instructions. Algorithms the logical sequence of determined operations that allows a problem to be solved mathematically.

What happens at the intersection of data and design? This question was the inspiration behind a process for innovation called Fully Integrated Thinking™, or FIT. One of the interesting data-design projects it's The FIT is an approach which is the intersection of data and design. Currently being further developed by a global collaboration of designers, biologists, Architects and other partners, the FIT "Fully Integrated Thinking" process identifies the questions we need to ask of our work to achieve more sustainable outcomes.

The FIT framework enables us to tap into the wisdom behind the natural, social and ecological systems of a place to inform design and decision-making. It allows us to find answers to today's design challenges by emulating 3.8 billion years of nature's genius (http://www.hok.com/thought-leadership/fully-integrated-thinking/).

Material-Based Design

One of the new approaches in architecture and design is the Material-based Design Computation is developed and proposed as a set of computational strategies supporting the integration of form, material and structure by incorporating physical form-finding strategies with digital analysis and fabrication. In this approach, material precedes shape, and it is the structuring of material properties as a function of structural and environmental
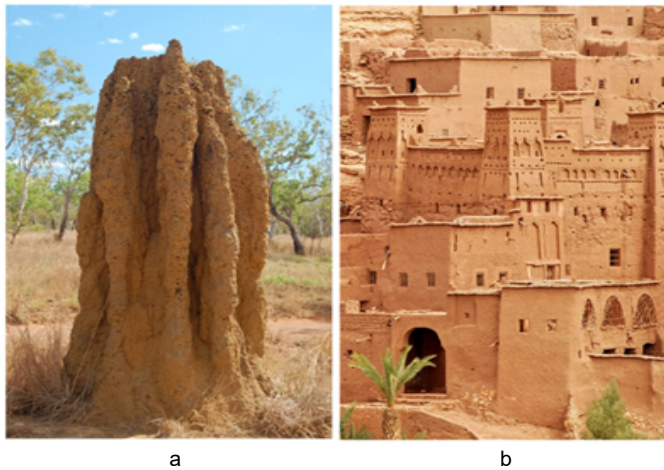
Figure 10. a – Termite Hill, Namibia, b – Ksar Ait Benhaddou, built from clay material as the Termite Hill (The formal similarity)
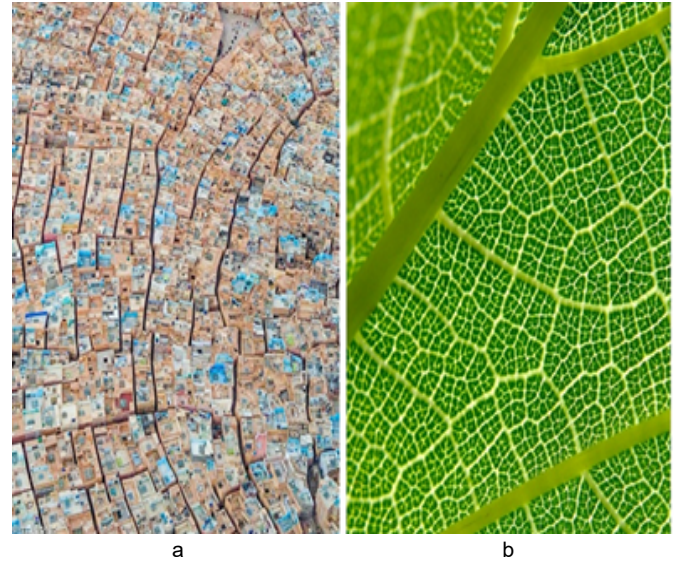

Figure 11. a – The road system of Ghardaia city, b – The leaf of tree (The functional similarity).

performance that generates design form. Material-based Design is a unique approach to computationally-enabled form-finding procedures, and experimentally investigates how such processes contribute to novel ways of creating, distributing and depositing material forms. The architects or designers are now able to establish parametric relationships between features, methods, and functions in a way that supports design processes of a generative nature (Oxman, 2010).

Material based Design Computation promotes an integrated approach to design, whereby material properties inform the geometric generation of highly complex 3-D surface structures, However, geometrical considerations, mainly, currently drive this liberation, which seems to be manifesting itself across the board throughout the continuous phases of the design process. Generative performative modelling approaches have been introduced that engage principles of engineering with form finding (Nori Oxman, 2009).

For computational design strategies there's too many new developments in digital fabrication, particularly in robotics fields, allow for the implementation of design principles such as heterogeneity, hierarchy, or anisotropy in architecture, which are characteristic principles found in nature. One of the examples, the fabrication of ultra-lightweight timber shells in architecture. Specifically, a robotic sewing method is developed in conjunction with a computational design method for the development of a new construction system that was evaluated through a large-scale prototype building (Tobias Schwinn, Oliver David Krieg, Achim Menges, 2016).

In recent years there are many sustainable policies with the desire to develop architecture and environmentally friendly designs and the protection of the environment, starting by the sustainable development for several regions of the world, one of them the great Sahara region is one of the most impressive places, by her architectural heritage and her environments, and contains hundreds of old and new cities.

Ecological Innovation of Saharan architecture by Biomimicry

With the rapid evolution of the architectural and urban language and the technological acceleration in the field of architecture and facing to the crisis in the new architecture and urbanism, the Saharan cities are recently part of a sustainable policy with the desire to develop the architecture and protect the environment, conserve its biodiversity and encourage sustainable development. The past examples can be a great source of inspiration about the demarche of the processes of conception in the architectural project in the Saharan cities which have a great heritage of architecture, and their cities always represented the concept of ecology and the respect of the environment, more than that, it's can be a soil favourable to great changes.

Traditional architecture in Saharan was based in the design buildings on natural materials and to design passively, the architectural styles and constructions technique are so various as the numerous influences that had inspired them.

The past examples can be a great source for inspiration about the demarche of the processes of conception in the architectural project in the Saharan cities which have a great heritage of architecture, and their cities was always represented the concept of ecology and the respect of the surrounding environment. The architectural styles are so various as the numerous influences that had inspired them.

For all the old population, nature was the first way of inspiration and a great way of understanding how things should be and how things should work, the Vernacular architecture is an example of an architecture which adapts to harsh climatic conditions, and which is born from nature and build by the using of natural material (Figure 10) and which represent the basic form of the Biomimicry approach but this architecture didn't develop with time and with the new needs.
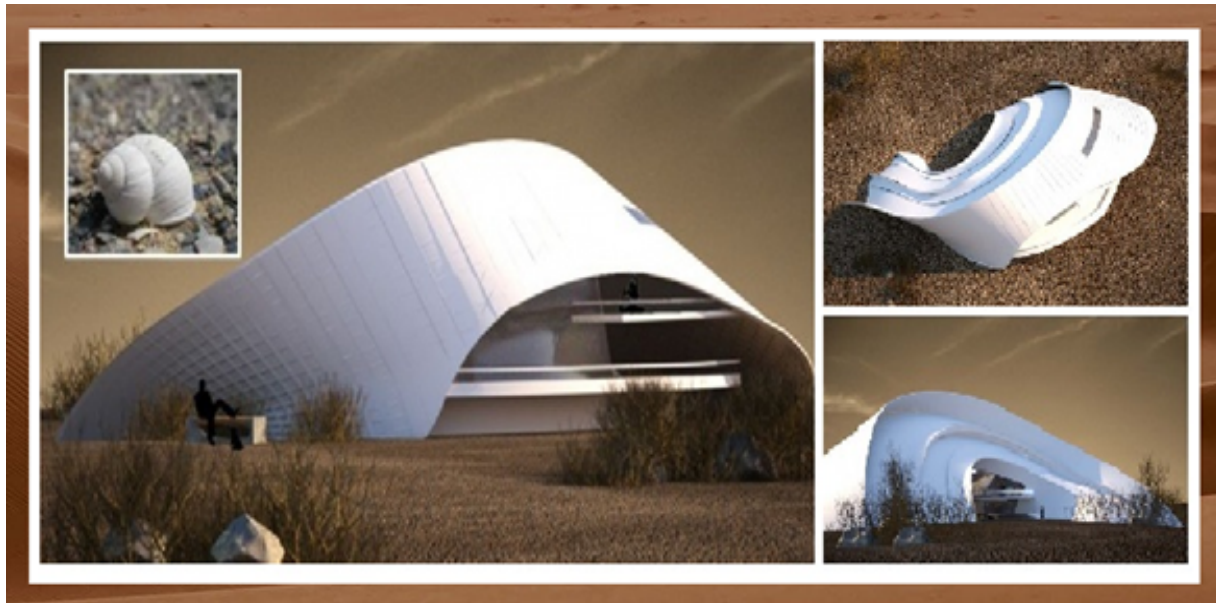
Figure 12. Curvy Desert Home Designed by Iranian Students Mimics the Snail
(https://www.greenprophet.com/2012/03/iran-desert-mimics-snail/)

The desert construction has always been effective in terms of adaptation to the harsh conditions of the terrain and climate. The cities are made in the forms of traditional architecture and natural materials largely due to the influence of the surrounding environment. Houses are compact with a closed outer face. The layout is similar in most of the villages (De Filippi, 2006) this layout of roads are based on tree system as shown below (Figure 11).

Under the pressure and the architectural crisis and the accelerated urbanization in the Saharan cities and the imperatives of sustainable development, the problems of the design of the projects and the modes of management and climate adaptation are strongly imposed. The new urban and architectural projects that exist in the Saharan context in the desert cities of North Africa are very reliable in terms of energy efficiency and in terms of the relationship between buildings and nature, According to Christophe Menezo (INSA / EDF), buildings consume 50% of energy resources. And many architects like Frei Otto consider that it is time to demand lighter architecture, more energy efficient, more mobile and more adaptable buildings, more natural buildings, without neglecting the demand for security. The new technologies, like 3D printers, BIM, the algorithms, open up new possibilities and the best innovation in the field of architecture.

The development of the Biomimicry approach takes us for more understanding of how important and interesting to refer nature to the design of an architectural project in a specific context. As a first departure, the relationship with nature is essential and the morphogenesis of the living allows us to understand what were the first fruits of the contributions of biology to architecture. Also aims to facilitate the transfer of knowledge from biology to other disciplines in order to solve technological or governance challenges (Menga, Monnier, 2014). However, the presumed technological and ecological advances are such that the world of Biomimicry and its international actors are now structured, attributing to this new approach a scale characterized by some of the "third industrial revolution" (Iswann, 2018).

The integration of Biomimicry in the innovation strategies of Saharan architecture and urbanism an urgent need to develop and solve engineering and environmental problems.

The future new Biomimicry project of architects and designers can demonstrate the vast potential of traditional architecture, combined with modern design and technologies, materials and construction techniques. we can mention a project which makes by a team of Iranian students "Art University of Isfahan" won a prestigious design competition with this biomimetic dwelling, this curvy desert dwelling, Like the snail, which retreats far into the depths of its shell when the weather is hot, we can mark here that the snail has remarkable qualities that have allowed it to stay both cool and moist in even the harshest temperatures.

For the design team found its form, the material of its shell, and its coping strategies to be qualities worth emulating in architecture (Laylin, 2012). The imitation of form and function of a snail results in a functional, innovative, and energy-efficient architecture that sustains in the hottest temperature of the desert.

We have described the methods proposed for Biomimicry with projects that enriched and showed that there are several possible attitudes for bio-inspiration in architecture and in biomimetic methods, as a rapid development and an innovate approach in which the architect participates in the biomimetic activity in collaboration with biologists and computer scientists.

The use of the Biomimicry approach can take us for more understanding of how important and interesting to refer nature to the design of an architectural project, the relationship to nature is essential and can start by the transfer of knowledge from biology to other disciplines

in order to solve technological or governance challenges (David Menga, Bernard Monnier, 2014). The integration of Biomimicry in the innovation strategies of Saharan architecture and urbanism an urgent need to develop and solve engineering and environmental problems, the future new Biomimicry project of architects and designers can demonstrate the vast potential of traditional architecture, combined with modern design and technologies, materials and construction techniques.

The biomimetic design methodology capable of producing innovations for Saharan architecture in order to answer the sustainable development issues. The main objective of this article was to present a synthesis of the approach to design and approaches based on Biomimicry and can be a great option for the optimal sustainable development of the desert cities, there are many tools or methods to operationalize the biomimetic approach. Biomimicry certainly offers methods and approaches based on the world of nature but Also the proposed biomimetic approach of solutions also conform to economic, management, social, technological, and technical expectations.

Conclusion

The inspiration by Nature's is the most optimal strategies which give us an architecture with maximal performance and in the same time with minimal resources without energy wasting. Today, under the imperatives and the intensive growing of the failures and environmental liabilities of the Biomimetic approach, with high performance and exceedingly effective and efficient structures.

For the using of biomimetic approach and the innovation of traditional architecture, firstly we propose the creation of a digital platform with collaboration between architects, biologists, computer scientists, engineers, this platform it's necessary with providing several assistance tools, based on algorithms as well as tools for decision support as the optimization and modulization, and creations of punctual projects in the cities and develop a strategies of an biomimetic renovation of the traditional cities based on a biomimetic approaches

The biomimetic design process from the natural morphogenesis to project design can be as the following step:

1. Identify problems or needs.
2. Determination of the biological basis based on the result of the project requirement or the problem.
3. The abstraction of the results.
4. The modulization and simulation of the model.
5. The Implementation.

The aim of this theoretical work is to explain biomimicry methods and process that have a positive impact on the environment and architecture development, we can be sure that in the field of architecture, the bio-inspiration has a great of potential point to meet the current challenges of designing efficient for forms or structures, energy efficiency and climate and optimization of flows at the urban conditions and many other parameters. The challenge for the coming years is the development of an intelligent platform which can make all this steps based on the database of the behaviour or the form or ecosystem of all organism in nature and give us the most optimal solutions for many problem and innovation design in Sahara.

We can say that the Biomimicry can be as a Renaissance for the Saharan architecture, and for her sustainable development

References

Barlovatz-Meimon, G., Sené, S. (2018). *Méthodes informatiques en biologie [Computer Methods in Biology]*. Lyon: Institut Rhônealpin des systèmes complexes (IXXI), pp. 1–3.

Benyus, J. (2011). *Biomimétisme: Quand la nature inspire des innovations durables [Biomimicry: When nature inspires sustainable innovations]*. Paris: Rues de l'échiquier. (in French)

Carr, J. (2014). *An Introduction to Genetic Algorithms.* Available at: https://www.whitman.edu/Documents/Academics/Mathematics/2014/carrjk.pdf. (accessed on 12.09.2018)

Chayaamor-Heil, N., Guéna et Nazila Hannachi-Belkadi, F. (2018). B*iomimicry in Architecture: State, methods and tools*. Available at: https://journals.openedition.org/craup/309. (accessed on 12.09.2018) (in French)

De Filippi, F. (2006). Traditional architecture in the Dakhleh Oasis, Egypt: space, form and building systems. In: *Proceedings of The 23rd Conference on Passive and Low Energy Architecture*. Geneva: PLEA2006, pp. 1–6.

Iswann, A. B. (2018). V*ers la ville biomimétique, Quand la nature inspire le développement urbain durable [Towards the Biomimetic City, When Nature Inspires Sustainable Urban Development]*. Available at: http://www.masterbioterre.com/sites/default/files/Vers%20la%20ville%20biomim%C3%A9tique%20Ali%20Benali.pdf. (accessed on 12.09.2018) (in French)

Laylin, T. (2012). *Curvy Desert Home Designed by Iranian Students Mimics the Snail*. Available at: https://www.greenprophet.com/2012/03/iran-desert-mimics-snail/. (accessed on 12.09.2018)

Madjer, K. (2014). *Le métro de Tokyo et les routes des États-Unis modélisés par un micro-organisme [Tokyo subway and US roads modeled by a microorganism]*. Available at: http://sweetrandomscience.blogspot.ru/2014/01/le-metro-de-tokyo-et-les-routes-des.html. (accessed on 12.09.2018) (in French)

Menga, D., Monnier, B. (2014). *Le biomimétisme, Comment la nature nous aide à innover [Biomimicry, How nature helps us to innovate]*. Palaiseau: École Polytechnique. (in French)

Oxman, N. (2009). *Material-Based Design Computation: Tiling Behavior, Computation Group, Department of Architecture, Massachusetts Institute of Technology.* Available at: http://papers.cumincad.org/data/works/att/acadia09_122.content.pdf. (accessed on 07.10.2018)

Oxman, N. (2010). *Material-based Design Computation.* Massachusetts: Massachusetts Institute of Technology.

Rao, R. (2014). Biomimicry in Architecture. *International Journal of Advanced Research in Civil, Structural, Environmental and Infrastructure Engineering and Developing,* 1 (3), pp. 101–107.

Raskin, K., Cruz, E. (2017). *Architecture bio-inspirée : vers la conception d'habitats régénératifs [Bio-inspired Architecture: Towards Regenerative Habitat Design]*. Available at: http://anabf.org/pierredangle/magazine/europe-et-international/architecture-bio-inspiree-vers-la-conception-dhabitats-r-g-n-ratifs. (accessed on 12.09.2018) (in French)

Schwinn, T., Krieg, O.D., Menges, A. (2016). Robotic Sewing "A Textile Approach Towards the Computational Design and Fabrication of Lightweight Timber Shells". Available at: http://papers.cumincad.org/data/works/att/acadia16_224.pdf. (accessed on 07.10.2018)

Stals, A. (2013). *Nature et architecture, De la morphogenèse du vivant à la création numérique [Nature and architecture, From the morphogenesis of the living to the digital creation]*. Liège: University of Liège. (in French)

URBEO (2010). *Eco-urbanisme, le Biomimétisme une source pour l'architecture durable, recherche et perspective [Eco-urbanism, Biomimicry a source for sustainable architecture, research and perspective]*. Available at: https://ru.calameo.com/read/002595223b76153823070 (accessed on 12.09.2018) (in French)

ELASTICITY ANISOTROPY OF COMPOSITES

Vladimir Glukhikh

Saint Petersburg State University of Architecture and Civil Engineering
Vtoraja Krasnoarmejskaja ul., 4, St. Petersburg, 190005, Russia

VNGlukhikh@mail.ru

Abstract

The article presents a solution to a problem on the establishment of mathematical relations between elastic constants of anisotropic fiber composites in principal anisotropy directions. A stress function in the form of a polynomial sum was used to solve the fourth-order differential equation in partial derivatives for an orthotropic body, thus allowing determining elastic constants of fiber composites with different directions of reinforcing fibers by means of mathematical calculations. It was established that all anisotropic materials could be conditionally divided into two groups.

One group includes composites in which elastic constants take an intermediate extreme value at 60° upon change of the reinforcing fibers position from 0 to 90°. The other group includes composites with two extreme values — at 0 and 90°. This new knowledge obtained for the first time shall be used to provide rationale for the method of composite strength assessment by means of calculations depending on the position of reinforcing fibers, which was previously possible only upon execution of experimental studies.

Keywords

Composite materials, elastic constants, anisotropy, fiber materials, filament-wound materials, principal directions, orthotropic body.

Introduction

Evolution of living systems and vegetable origin systems is accompanied by optimization of their "engineering" components with the following improvement of resistance to external impacts. An ordered structure (17) forms under the influence of the environment.

The strongest reinforcing fibers formed in mechanical tissues during evolutionary optimization of bearing structures. The direction of such fibers coincides with maximum tensile and compressive stresses.

Micro- and macro-structure orientation providing high resistance of mechanical tissues to external impacts represents a result of evolutionary optimization of support systems in nature, including bone tissues of animals and humans, plant and tree stems. In recent decades, such ordered structure of mechanical tissues in the plant, animal and human world has become an object of increasing attention with the purpose of borrowing when developing new high-strength composites for engineering and construction — materials with pre-defined properties.

In a relatively short period of time, composites have evolved from materials designed exclusively for strategic and military use to wide application materials used in various industries and national economy sectors.

Due to the increasing demand of population in many countries for the wide range of residential buildings, special attention is given to application of new advanced high-performance composites with high aesthetic, as well as special characteristics, intended to be used in construction.

For more than one decade, composites with a structure reminding the tree stem have been made by winding (with the use of reinforcement made of fiber metal and non-metal materials in the form of fibers or strips (16)).

In many cases, filament-wound composites can be referred to cylindrically anisotropic materials. The full set of characteristics of their elastic stress-strain behavior includes nine independent elastic constants (Ashkenazi, 1978; Lekhnitsky, 1977).

Knowing values of elastic constants in principal anisotropy directions, we can determine the value of any elastic constant in the required direction, which is often necessary when determining deformations in directions not coinciding with principal ones (Ashkenazi, 1978; Ashkenazi et al., 1981; Lekhnitsky, 1957).

To determine values of elastic constants in any directions, we can use equations suggested by S.G. Lekhnitsky (1957), Ye.K. Ashkenazi (1978, 1981), A.N. Mitinsky (1948, 1949) and other scientists. Those equations include experimentally found elastic constants in principal anisotropy directions. The authors also paid special attention to the inclusion of the shear and elastic moduli, as well as the Poisson's ratio in directions at the angle of 45° in relation to reinforcing fibers, the method of determination of which is imperfect, according to the authors. This is due to the lack of mathematical relations between elastic constants in principal anisotropy directions like in isotropic materials. This paper suggests a way to improve the method for determination of elastic constants in filament-wound composites by establishment of mathematical relations between their elastic constants in principal anisotropy directions.

Research method

As a basis of the theoretical research, a fourth-order differential equation in partial derivatives (known in the theory of elasticity of an anisotropic body) for a cylindrically anisotropic orthotropic body, in polar coordinates, which the stress function satisfies, was taken. Without consideration of body forces, this equation in polar coordinates is written as follows (Ashkenazi, 1978; Lekhnitsky, 1957, 1977):

$$\frac{1}{E_t}\cdot\frac{\partial^4 F}{\partial r^4}+\left(\frac{1}{G_{rt}}-\frac{2\mu_{rt}}{E_r}\right)\cdot\frac{1}{r^2}\cdot\frac{\partial^4 F}{\partial r^2\partial\theta^2}+\frac{1}{E_r}\cdot\frac{1}{r^4}\cdot$$

$$\cdot\frac{\partial^4 F}{\partial\theta^4}+\frac{2}{E_t}\cdot\frac{1}{r}\cdot\frac{\partial^3 F}{\partial r^3}-\left(\frac{1}{G_{rt}}-\frac{2\mu_{rt}}{E_r}\right)\cdot\frac{1}{r^3}\cdot\frac{\partial^3 F}{\partial r\partial\theta^2}-$$

$$-\frac{1}{E_r}\cdot\frac{1}{r^2}\cdot\frac{\partial^2 F}{\partial r^2}+\left(2\frac{1-\mu_{rt}}{E_r}+\frac{1}{G_{rt}}\right)\cdot\frac{1}{r^4}\cdot\frac{\partial^2 F}{\partial\theta^2}+$$

$$+\frac{1}{E_r}\cdot\frac{1}{r^3}\cdot\frac{\partial F}{\partial r}=0$$

(1)

It is convenient to use the obtained equation for circular plates. To solve tasks related to design of rectangular

elements, it is more convenient to use the last equation in Cartesian coordinates.

After differentiation and substitution of the corresponding derivatives in equation (1), the following fourth-order differential equation in partial derivatives in Cartesian coordinates is obtained for a cylindrically anisotropic orthotropic body:

$$\frac{\partial^4 F}{\partial x^4}(x^4+Bx^2y^2+\alpha^2y^4)+\frac{\partial^4 F}{\partial y^4}(y^4+Bx^2y^2+\alpha^2x^4)+$$

$$+\frac{\partial^4 F}{\partial y\partial x^3}\left[2x^2+B(y^2-x^2)-2\alpha^2y^2\right]\cdot 2xy+\frac{\partial^4 F}{\partial x\partial y^3}\cdot$$

$$\cdot\left[2y^2+B(x^2-y^2)-2\alpha^2x^2\right]\cdot 2xy+\frac{\partial^4 F}{\partial x^2\partial y^2}\cdot$$

$$\cdot\left[6x^2y^2+B(x^4-4x^2y^2+y^4)+6\alpha^2x^2y^2\right]+\frac{\partial^3 F}{\partial x^3}$$

(2)

$$\cdot\left[2x^2+B(3y^2-x^2)-6\alpha^2y^2\right]\cdot x+\frac{\partial^3 F}{\partial y^3}\cdot$$

$$\cdot\left[2y^2+B(3x^2-y^2)-6\alpha^2x^2\right]\cdot y+\frac{\partial^3 F}{\partial y\partial x^2}\cdot$$

$$\cdot\left[2x^2(1+2\alpha^2)+B(y^2-3x^2)-2\alpha^2y^2\right]\cdot 3y+\frac{\partial^3 F}{\partial x\partial y^2}$$

$$\cdot\left[2y^2(1+2\alpha^2)+B(x^2-3y^2)-2\alpha^2x^2\right]\cdot 3x+$$

$$+\frac{\partial^2 F}{\partial x^2}(2\alpha^2-B)(x^2-y^2)+\frac{\partial^2 F}{\partial y^2}(B-2\alpha^2)\cdot$$

$$\cdot(x^2-y^2)+\frac{\partial^2 F}{\partial x\partial y}(2\alpha^2-B)\cdot 4xy=0$$

where $\alpha^2=\dfrac{E_t}{E_r}$; $B=E_t\left(\dfrac{1}{G_{rt}}-\dfrac{2\mu_{rt}}{E_r}\right)$ (3)

If the load on edges and ends of a rectangular anisotropic plate is set in the form of an entire algebraic function, then the corresponding stress function can be taken in the form of an entire polynomial. The task is solved using the stress function in the form of a sum of polynomials (Kurdyumov, 1946; Glukhikh, 2001, 1997, 2007, 2008, 2009):

$$F_{(x.y)}=\sum_{k=1}^{N}f_k(y)x^k$$

(4)

where $f_k(y)$ — a function unknown at the initial solution stage, that shall satisfy differential equation (Ashkenazi, Ganov, 1981) and conditions on the plate contour.

The stress function is taken in the form of the following sum of polynomials (Kurdyumov, 1946; Glukhikh, 2001):

$$F(x,y)=f_0(y)+xf_1(y)+x^2f_2(y)+x^3f_3(y)+x^4f_4(y)+$$

$$+x^5 f_5(y) + x^6 f_6(y) + x^7 f_7(y) + x^8 f_8(y) + x^9 f_9(y) \qquad (5)$$

The corresponding derivatives of the stress function $F(x, y)$ are substituted in differential equation (2).

If we equate factors multiplying the corresponding x degrees to zero, we will obtain differential equations that the selected stress function shall satisfy. The first group of equations will include functions $f_k(y)$ with even numbers only, including $f_0(y)$. The second group of equations will include functions $f_k(y)$ with odd numbers.

The first group of equations is as follows:

$$24\alpha^2 y^4 f_4(y) + 2B y^4 f_2''(y) + 6(B - 2\alpha^2)y^3 f_2'(y) +$$
$$+2(B - 2\alpha^2)y^2 f_2(y) + y^4 f_0^{IV}(y) + (2 - B)y^3 f_0'''(y) - \qquad (6)$$
$$-(B - 2\alpha^2)y^2 f_2''(y) = 0$$

$$360\alpha^2 y^4 f_6(y) + 12B y^4 f_4''(y) + 84(B - 2\varepsilon^2)y^3 f_4'(y) +$$
$$+(108B - 168\alpha^2)y^2 f_4(y) + 5(2 - B)y^3 f_2'''(y) + (24 -$$
$$-27B + 38\alpha^2)y^2 f_2''(y) + (12 + 40\alpha^2 - 26B)yf_2'(y) + \qquad (7)$$
$$-2(B - 2\alpha^2)f_2(y) + By^2 f_2^{IV}(y) + 3(B - 2\alpha^2)yf_0'''(y) +$$
$$+(B - 2\alpha^2)f_0''(y) = 0$$

$$1680\alpha^2 y^4 f_8(y) + 30B y^4 f_6''(y) + 330(B - 2\alpha^2)y^3 f_6'(y) +$$
$$+(750B - 780\alpha^2)y^2 f_6(y) + y^4 f_4^{IV}(y) + 9(2 - B)y^3 f_4'''(y) +$$
$$+(96 + 122\alpha^2 - 85B)y^2 f_4''(y) + (168 - 172B + 176\alpha^2)yf_4'(y) + \qquad (8)$$
$$+12(6 - 3B - 2\alpha^2)f_4(y) + By^2 f_2^{IV}(y) + 7(B - 2\alpha^2)yf_2'''(y) +$$
$$+(9B - 14\alpha^2)f_2''(y) + \alpha^2 f_0^{IV}(y) = 0$$

When using stress function components $(f_{10}(y), f_{12}(y),$ …$)$, equations following equation (8) form in the group, including $f_{10}(y), f_{12}(y)$, etc., respectively.

It should be noted that all functions newly appearing in equations (7), (8), etc. will be related to $f_0(y), f_2(y), f_4(y)$ as per equation (6).

The second group of equations is as follows:

$$120\alpha^2 y^4 f_5(y) + 6B y^4 f_3''(y) + 30(B - 2\alpha^2)y^3 f_3'(y) +$$
$$+24(B - 2\alpha^2)y^2 f_3(y) + y^4 f_1^{IV}(y) + 3(2 - B)y^3 f_1'''(y) + \qquad (9)$$
$$+2(3 + 7\alpha^2 - 5B)y^2 f_1''(y) - 4(B - 2\alpha^2)yf_1'(y) = 0;$$

$$840\alpha^2 y^4 f_7(y) + 20B y^4 f_5''(y) + 180(B - 2\alpha^2)y^3 f_5'(y) +$$
$$(320B - 400\alpha^2)y^2 f_5(y) + y^4 f_3^{IV}(y) + 7(2 - B)y^3 f_3'''(y)$$
$$+(54 - 52B + 74\alpha^2)y^2 f_3''(y) + (60 + 96\alpha^2 - 78B)yf_3'(y) + \qquad (10)$$
$$+121 + \alpha^2 - B()f_3(y) + By^2 f_1^{IV}(y) + 5(B - 2\alpha^2)yf_1'''(y) +$$
$$+4(B - 2\alpha^2)f_1''(y) = 0;$$

$$3024\alpha^2 y^4 f_9(y) + 42B y^4 f_7''(y) + (546B - 1092\alpha^2)y^3 f_7'(y) +$$
$$+(1512B - 1344\alpha^2)y^2 f_7(y) + y^4 f_5^{IV}(y) + 11(2 - B)y^3 f_5'''(y) + \qquad (11)$$
$$+(150 + 182\alpha^2 - 126B)y^2 f_5''(y) + (360 + 280\alpha^2 - 320B)yf_5'(y) +$$
$$+(240 + 40\alpha^2 - 80B)f_5(y) + By^2 f_3^{IV}(y) + 9(B - 2\alpha^2)yf_3'''(y) +$$
$$+(16B - 20\alpha^2)f_3''(y) + \alpha^2 f_1^{IV}(y) = 0;$$

Here the same pattern as in the previous case manifests itself. When using additional functions $f_{11}(y)$, $f_{13}(y)$, etc., differential equations following equation (11) form, including $f_{11}(y), f_{13}(y)$, etc., respectively.

All functions $f_7(y), f_9(y)$, etc. are dependent on functions $f_1(y), f_3(y)$ and $f_5(y)$ as per (9).

Thus, a task with any number of functions $f_k(y)$ can be solved in the following way: at the first stage, functions $f_0(y), f_1(y), …, f_5(y)$ are determined based on equations (6) and (9), and then the remaining functions are determined.

Considering the order of derivatives $f_k^{(n)}(y)$ and degree of variable y, the solution of homogeneous differential equations (6)–(11) with variable coefficients can be represented in the form of algebraic functions:

$$f_k(y) = C_0 + C_1 y + C_2 y^2 + C_3 y^3 + C_4 y^4 + … \qquad (12)$$

where C — integration constants.

Using the stress function $F(x, y)$ in the form of a sum of polynomials for solution of differential equations (6)–(11), we can assume a relation between integration constants. This inevitably derives from the requirement for satisfaction of those differential equations with the selected function $F(x, y)$.

Let us use, for example, the following stress function at the first stage:

$$F(x, y) = f_0(y) + x^2 f_2(y) + x^4 f_4(y) + x^6 f_6(y) + x^8 f_8(y) \qquad (13)$$

and differential equation (8); in order for $F(x, y)$ to satisfy differential equation (8), it is required to accept the following:

$$f_8(y) = C_{81} + C_{82}y + C_{83}y^2 + C_{84}y^3 \qquad (14)$$

$$f_6(y) = C_{61} + C_{62}y + C_{63}y^2 + C_{64}y^3 + C_{65}y^4 + C_{66}y^5 \qquad (15)$$

$$f_4(y) = C_{41} + C_{42}y + C_{43}y^2 + C_{44}y^3 + C_{45}y^4 + C_{46}y^5 + C_{47}y^6 + C_{48}y^7 \qquad (16)$$

$$f_2(y) = C_{21} + C_{22}y + C_{23}y^2 + C_{24}y^3 + C_{25}y^4 + C_{26}y^5 +$$
$$+C_{27}y^6 + C_{28}y^7 + C_{29}y^8 + C_{210}y^9 \qquad (17)$$

$$f_0(y) = C_{01} + C_{02}y + C_{03}y^2 + C_{04}y^3 + C_{05}y^4 + C_{06}y^5 +$$
$$+C_{07}y^6 + C_{08}y^7 + C_{09}y^8 + C_{010}y^9 + C_{011}y^{10} + C_{012}y^{11} \qquad (18)$$

Substituting these functions and their corresponding derivatives in differential equation (6), and equating factors multiplying the corresponding y degrees to zero, the following correlations between integration constants can be obtained:

$$C_{21} = C_{03} \qquad (19)$$

$$C_{22} = C_{04}\frac{3(B - 1 - \alpha^2)}{2(B - 2\alpha^2)}; etc. \qquad (20)$$

Performing similar rearrangements with the use of functions (14)–(18) and differential equation (7), new correlations between arbitrary constants can be obtained:

$$C_{03} = C_{21} \qquad (21)$$

$$C_{22} = -C_{04} \frac{6(B - 2\alpha^2)}{3 + 11\alpha^2 - 7B} \tag{22}$$

Let us perform similar rearrangements with the use of equations (14)–(18) and (8).

A similar solution can be achieved for three differential equations (9), (10) and (11) involving functions with odd numbers $f_1(y)$, $f_3(y)$, $f_5(y)$, $f_7(y)$, represented in the following form:

$$f_9(y) = C_{91} + C_{92}y + C_{93}y^2 + C_{94}y^3 \tag{23}$$

$$f_7(y) = C_{71} + C_{72}y + C_{73}y^2 + C_{74}y^3 + C_{75}y^4 + C_{76}y^5 \tag{24}$$

$$f_5(y) = C_{51} + C_{52}y + C_{53}y^2 + C_{54}y^3 + \\ + C_{55}y^4 + C_{56}y^5 + C_{57}y^6 + C_{58}y^7; \tag{25}$$

$$f_3(y) = C_{31} + C_{32}y + C_{33}y^2 + C_{34}y^3 + C_{35}y^4 + \\ + C_{36}y^5 + C_{37}y^6 + C_{38}y^7 + C_{39}y^8 + C_{310}y^9 \tag{26}$$

$$f_1(y) = C_{11} + C_{12}y + C_{13}y^2 + C_{14}y^3 + C_{15}y^4 + C_{16}y^5 + \\ + C_{17}y^6 + C_{18}y^7 + C_{19}y^8 + C_{110}y^9 + C_{111}y^{10} + C_{112}y^{11} \tag{27}$$

Substituting (23)–(27) to (9) and performing rearrangements, we will obtain the following:

$$C_{12} = 0 \tag{28}$$

according to the task condition for stresses, $C_{11}=0$ shall be taken:

$$C_{31} = -C_{13} \frac{3 + 11\alpha^2 - 7B}{6(B - 2\alpha^2)} \tag{29}$$

Similar correlations between integration constants can be obtained after rearrangement of equation (8) considering (23)–(27):

$$C_{31} = -C_{13} \frac{2(B - 2\alpha^2)}{3(1 + \alpha^2 - B)} \tag{30}$$

Analyzing equation (22) at this stage when the integration constants are unknown, we shall note that the constant C_{04} does not become zero upon solution of bending problems. It is known that in case of an isotropic body, the law of normal stress distribution by cross-sectional height upon bending is linear.

Elastic properties of isotropic bodies are defined by three characteristics, two of which are independent:

$$G = \frac{E}{2(1 + \mu)} \tag{31}$$

As noted above, a similar correlation should exist for a cylindrically anisotropic body.

Upon solution of differential equation (2) in Cartesian coordinates with application of the stress function in the form of a sum of polynomials (4), it was established that correlations between integration constants depended on elastic constants. This holds in equation (3).

Correlations (20) and (22) between the constants C_{22} and C_{04} come under notice.

It was noted above that the constant C_{04} does not become zero, therefore, the constant C_{22} is not equal to zero as well. Let us equate factors multiplying C_{04} in the right parts of equations (20) and (22) to each other:

$$\frac{3(B - 1 - \alpha^2)}{2(B - 2\alpha^2)} = -\frac{6(B - 2\alpha^2)}{3 + 11\alpha^2 - 7B} \tag{32}$$

The same can be performed for factors multiplying the constants C_{31} and C_{13} in correlations (29) and (30).

As a result of the rearrangement, equation (32) takes the following form:

$$B^2 - \frac{2}{3}(5 + \alpha^2)B - \frac{5}{3}\alpha^4 + \frac{14}{3}\alpha^2 + 1 = 0 \tag{33}$$

where the roots of the equation are:

a) $B_{(1)} = \dfrac{1 + 5\alpha^2}{3}$; b) $B_{(2)} = 3 - \alpha^2$ \hfill (34)

Results

Based on (3), the shear modulus can be calculated:

$$G_{rt} = \frac{E_t}{B + 2\mu_{tr}} \tag{35}$$

which, considering (35), will be represented by the following:

$$B < 2 \,; \; G_{rt} = \frac{3E_t}{1 + 5\alpha^2 + 6\mu_{tr}} \tag{36}$$

$$B > 2 \,; \; G_{rt} = \frac{E_t}{3 - \alpha^2 + 2\mu_{tr}} \tag{37}$$

In case of an isotropic body, the last two equations will take the form of equation (31).

Results of equation (33) roots determination under different values of α^2 are presented in Table 1. This correlation is graphically represented in Figure 1.

Table 1. B values at different α^2 values

α^2	0.3	0.4	0.5	0.6	0.7	0.8
$B_{(1)} = \dfrac{1 + 5\alpha^2}{3}$	0.8333	1	1.1667	1.3333	1.5	1.6667
$B_{(2)} = 3 - \alpha^2$	2.7	2.6	2.5	2.4	2.3	2.2

Several differences between calculation results and some data (Ashkenazi, Ganov, 1981) are due to the fact that those data were obtained with the use of elasticity characteristics in the direction at the angle of 45° to principal anisotropy axes transverse to reinforcing
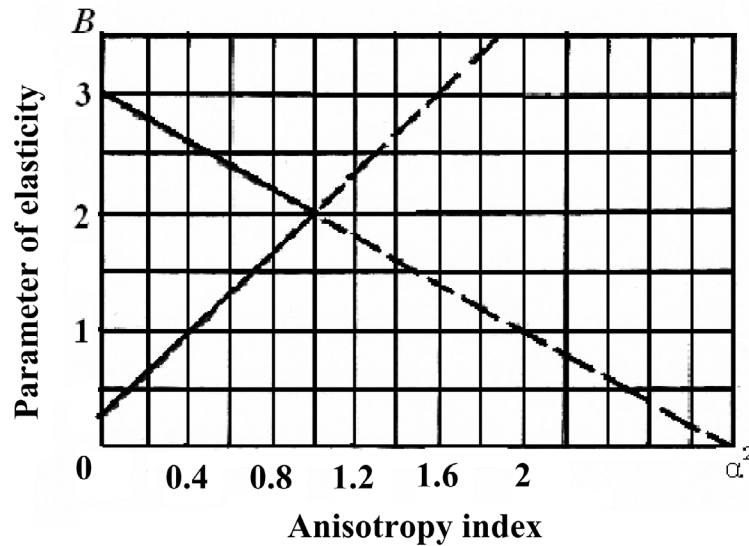
Figure 1. Changes in equation (33) roots depending on α^2.

fibers. According to the authors (Glukhikh, 2001), the method for experimental determination of these elasticity characteristics is imperfect.

We obtained results corresponding to relations between integration constants in differential equations (6)–(8). However, even with account for the fact that the methods for determination of elastic constants is imperfect, our calculations in most cases are quite close to the available data. In the example considered, this holds for the value of the equation root $B = 3-\alpha^2$.

It was theoretically confirmed that for an anisotropic body the value B can differ from 2 upward or downward (excluding $B = 2$ for an isotropic body).

With account for root (34, a) of algebraic equation (33), differential equation in polar coordinates (1) will take the following form (Glukhikh, 1998):

$$\frac{\partial^4 F}{\partial r^4} + \frac{1+5\alpha^2}{3} \cdot \frac{1}{r^2} \cdot \frac{\partial^4 F}{\partial r^2 \partial \theta^2} + \frac{\alpha^2}{r^4} \cdot \frac{\partial^4 F}{\partial \theta^4} + \frac{2}{r} \cdot$$
$$\frac{\partial^3 F}{\partial r^3} - \frac{1+5\alpha^2}{3} \cdot \frac{1}{r^3} \cdot \frac{\partial^3 F}{\partial r \partial \theta^2} - \frac{\alpha^2}{r^2} \cdot \frac{\partial^2 F}{\partial r^2} +$$
$$+ \frac{1+11\alpha^2}{3} \cdot \frac{1}{r^4} \cdot \frac{\partial^2 F}{\partial \theta^2} + \frac{\alpha^2}{r^2} \cdot \frac{\partial F}{\partial r} = 0$$

(38)

A similar solution (not given in the article) can be performed for a plane problem in displacements, using the differential equations obtained earlier.

The differential equations given above allow solving tasks related to cylindrically anisotropic orthotropic bodies, in which correlations between elastic constants in principal anisotropy directions, that are affected by roots (34, a) and (34, b) of algebraic equation (33).

For composites, in which the correlation between elastic constants in principal anisotropy directions is affected by law (37), differential equations can be written in the following form:
- in Cartesian coordinates:

$$\frac{\partial^4 F}{\partial x^4}\left(x^4 + \frac{1+5\alpha^2}{3}x^2 y^2 + \alpha^2 y^4 \right) + \frac{\partial^4 F}{\partial y^4} \cdot$$
$$\cdot \left(y^4 + \frac{1+5\alpha^2}{3}x^2 y^2 + \alpha^2 x^4 \right) + 2\frac{\partial^4 F}{\partial y \partial x^3} \cdot$$
$$\cdot \left[2x^2 + \frac{1+5\alpha^2}{3}(y^2 - x^2) - 2\alpha^2 y^2 \right] \cdot xy + 2\frac{\partial^4 F}{\partial x \partial y^3} \cdot$$

(39)

$$\cdot \left[2y^2 + \frac{1+5\alpha^2}{3}(x^2 - y^2) - 2\alpha^2 x^2 \right] \cdot xy + \frac{\partial^4 F}{\partial x^2 \partial y^2} \cdot$$
$$\cdot \left[6x^2 y^2 + \frac{1+5\alpha^2}{3}(x^4 - 4x^2 y^2 + y^4) + 6\alpha^2 x^2 y^2 \right] + \frac{\partial^3 F}{\partial x^3} \cdot$$
$$\cdot \left[2x^2 + \frac{1+5\alpha^2}{3}(3y^2 - x^2) - 6\alpha^2 y^2 \right] \cdot x + \frac{\partial^3 F}{\partial y^3} \cdot$$
$$\cdot \left[2y^2 + \frac{1+5\alpha^2}{3}(3x^2 - y^2) - 6\alpha^2 x^2 \right] \cdot y + 3\frac{\partial^3 F}{\partial y \partial x^2} \cdot$$
$$\cdot \left[2x^2(1+2\alpha^2) + \frac{1+5\alpha^2}{3}(y^2 - 3x^2) - 2\alpha^2 y^2 \right] \cdot y + 3\frac{\partial^3 F}{\partial x \partial y^2} \cdot$$
$$\cdot \left[2y^2(1+2\alpha^2) + \frac{1+5\alpha^2}{3}(x^2 - 3y^2) - 2\alpha^2 x^2 \right] \cdot x + \frac{\partial^2 F}{\partial x^2} \cdot$$
$$\cdot \frac{\alpha^2 - 1}{3} \cdot (x^2 - y^2) + \frac{\partial^2 F}{\partial y^2} \cdot \frac{1-\alpha^2}{3} \cdot (x^2 - y^2) +$$
$$+ \frac{4\partial^2 F}{3\partial x \partial y} \cdot (\alpha^2 - 1) \cdot xy = 0$$

- in polar coordinates (Glukhikh, 1998):

$$\frac{\partial^4 F}{\partial r^4} + (3 - \alpha^2) \cdot \frac{1}{r^2} \cdot \frac{\partial^4 F}{\partial r^2 \partial \theta^2} + \frac{\alpha^2}{r^4} \cdot \frac{\partial^4 F}{\partial \theta^4} + \frac{2}{r} \cdot$$

(40)

$$\cdot \frac{\partial^3 F}{\partial r^3} - (3 - \alpha^2) \cdot \frac{1}{r^3} \cdot \frac{\partial^3 F}{\partial r \partial \theta^2} - \frac{\theta^2}{r^2} \cdot \frac{\partial^2 F}{\partial r^2} +$$

17

$$+(3+\alpha^2)\cdot\frac{1}{r^4}\cdot\frac{\partial^2 F}{\partial\theta^2}+\frac{\alpha^2}{r^3}\cdot\frac{\partial F}{\partial r}=0$$

- in Cartesian coordinates:

$$\frac{\partial^4 F}{\partial x^4}\left[x^2(x^2+3y^2)+\alpha^2 y^2(y^2-x^2)\right]+\frac{\partial^4 F}{\partial y^4}\cdot$$

$$\cdot\left[y^2(y^2+3x^2)+\alpha^2 x^2(x^2-y^2)\right]+2\frac{\partial^4 F}{\partial x^3\partial y}(3y^2-x^2)\cdot(1-\alpha^2)\cdot$$

$$\cdot xy+2\frac{\partial^4 F}{\partial x\partial y^3}\cdot(3x^2-y^2)(1-\alpha^2)\cdot xy+\frac{\partial^4 F}{\partial x^2\partial y^2}\cdot$$

$$\cdot\left[2(5\alpha^2-3)x^2 y^2+(3-\alpha^2)(x^4+y^4)\right]+\frac{\partial^3 F}{\partial x^3}(1-\alpha^2)(9y^2-x^2)\cdot x+$$

$$+\frac{\partial^3 F}{\partial y^3}(1-\alpha^2)(9x^2-y^2)\cdot y+3\frac{\partial^3 F}{\partial y\partial x^2}(1-\alpha^2)(3y^2-7x^2)\cdot y+$$

$$+3\frac{\partial^3 F}{\partial x\partial y^2}(1-\alpha^2)(3x^2-7y^2)\cdot x+3\frac{\partial^2 F}{\partial x^2}(\alpha^2-1)(x^2-y^2)+$$

$$+3\frac{\partial^2 F}{\partial y^2}(1-\alpha^2)(x^2-y^2)+12\frac{\partial^2 F}{\partial y\partial x}(\alpha^2-1)\cdot xy=0$$

(41)

The full set of characteristics of elastic stress-strain behavior of orthotropic materials includes nine independent elastic constants subject to experimental determination. When determining deformation in an orthotropic material in the direction not coinciding with principal anisotropy axes, values of elastic constants in an arbitrary direction are required. Equations simultaneously including different elastic constants (Ashkenazi, 1978; Ashkenazi, Ganov, 1981; Lekhnitsky, 1957; Rabinovich, 1946) are required for calculation purposes:

$$\frac{1}{E_{x'}}=\frac{n_1^4}{E_x}+\frac{l_1^4}{E_y}+\frac{m_1^4}{E_z}+\left(\frac{1}{G_{xy}}-\frac{2\mu_{xy}}{E_x}\right)n_1^2 l_1^2+$$

$$+\left(\frac{1}{G_{yz}}-\frac{2\mu_{yz}}{E_y}\right)l_1^2 m_1^2+\left(\frac{1}{G_{zx}}-\frac{2\mu_{zx}}{E_z}\right)m_1^2 n_1^2$$

(42)

$$\frac{1}{G_{x'y'}}=4\left(\frac{n_1^2 n_2^2}{E_x}+\frac{l_1^2 l_2^2}{E_y}+\frac{m_1^2 m_2^2}{E_z}\right)-8\cdot$$

$$\cdot\left(\frac{\mu_{xy}}{E_x}n_1 n_2 l_1 l_2+\frac{\mu_{yz}}{E_y}l_1 l_2 m_1 m_2+\frac{\mu_{zx}}{E_z}m_1 m_2 n_1 n_2\right)+$$

$$+\frac{(n_1 l_2+l_1 n_2)^2}{G_{xy}}+\frac{(l_1 m_2+m_1 l_2)^2}{G_{yz}}+\frac{(m_1 n_2+n_1 m_2)^2}{G_{zx}}$$

(43)

$$\frac{\mu_{x'y'}}{E_{x'}}=-\frac{n_1^2 n_2^2}{E_x}-\frac{l_1^2 l_2^2}{E_y}-\frac{m_1^2 m_2^2}{E_z}+\frac{\mu_{xy}}{E_x}\left(n_1^2 l_2^2+n_2^2 l_1^2\right)+$$

$$\frac{\mu_{yz}}{E_y}\left(l_1^2 m_2^2+l_2^2 m_1^2\right)+\frac{\mu_{zx}}{E_z}\left(m_1^2 n_2^2+m_2^2 n_1^2\right)-$$

$$-\frac{n_1 n_2 l_1 l_2}{G_{xy}}-\frac{l_1 l_2 m_1 m_2}{G_{yz}}-\frac{m_1 m_2 n_1 n_2}{G_{zx}}$$

(44)

where n_1, n_2, ...m_1, m_2 — directional cosines.

Considering correlations (32) between elastic constants, equation (42) can be written for a cylindrically anisotropic orthotropic body in cylindrical coordinates:

$$\frac{1}{E_{x'}}=\frac{n_1^4}{E_r}+\frac{l_1^4}{E_t}+\frac{m_1^4}{E_a}+\frac{3-\alpha^2}{E_t}n_1^2 l_1^2+\left(\frac{1}{G_{ta}}-\frac{2\mu_{ta}}{E_t}\right)\cdot$$

$$\cdot l_1^2 m_1^2+\left(\frac{1}{G_{ar}}-\frac{2\mu_{ar}}{E_a}\right)m_1^2 n_1^2$$

(45)

– for the case when $B_{(2)} = 3 - \alpha^2$.
For an anisotropic material, in which elastic constants satisfy root (34), equation (45) takes the following form:

$$\frac{1}{E_{x'}}=\frac{n_1^4}{E_r}+\frac{l_1^4}{E_t}+\frac{m_1^4}{E_a}+\frac{1+5\alpha^2}{3E_t}n_1^2 l_1^2+$$

$$+\left(\frac{1}{G_{ta}}-\frac{2\mu_{ta}}{E_t}\right)l_1^2 m_1^2+\left(\frac{1}{G_{ar}}-\frac{2\mu_{ar}}{E_a}\right)m_1^2 n_1^2$$

(46)

Equations allowing determining the Poisson's ratios with account for new data (34, a, b) regarding elastic constants of a material with curvilinear anisotropy are as follows:
– for the anisotropy plane passing through axes *XY*:

$$\mu_{rt}=\frac{1}{2}\left[\frac{E_r}{E_t}+\frac{E_r}{G_{rt}}+1-\frac{4E_r}{E_{rt}^{(45)}}\right]$$

(47)

where $E_t/E_r=\alpha^2$; $G_{rt}^{\mathrm{I}}=\dfrac{3E_t}{1+5\alpha^2+6\mu_{tr}}$ from (36);

$G_{rt}^{\mathrm{II}}=\dfrac{E_t}{3-\alpha^2+2\mu_{tr}}$ from (37);

$E_{rt}^{(45)}=E_t$ from (45). Substituting (36), (37) and $E_{rt}^{(45)}$ to (47) and after rearrangements, the following is obtained for both options of a cylindrically orthotropic material:

$$\mu_{rt}=\frac{\mu_{rt}}{\alpha^2}$$

(48)

The obtained equation is in good agreement with the experimental data (Ashkenazi, Ganov, 1981).
– in two other (longitudinal) planes:

$$\mu_{ta}=\frac{1}{2}\left[\frac{E_t}{E_a}+\frac{E_t}{G_{ta}}+1-\frac{4E_t}{E_{ta}^{(45)}}\right]$$

(49)

$$\mu_{ar}=\frac{1}{2}\left[\frac{E_a}{E_r}+\frac{E_a}{G_{ar}}+1-\frac{4E_a}{E_{ar}^{(45)}}\right]$$

(50)

For the shear modulus upon rotation of axes in polar coordinates in the anisotropy plane perpendicular to the longitudinal axis with the use of (36):

$$\frac{1}{G_{x'y'}} = 4\left(\frac{n_1^2 n_2^2}{E_r} + \frac{l_1^2 l_2^2}{E_t} + \frac{m_1^2 m_2^2}{E_a}\right) - 8\left(\frac{\mu_{rt}}{E_r} n_1 n_2 l_1 l_2 + \frac{\mu_{ta}}{E_t} l_1 l_2 m_1 m_2 + \frac{\mu_{ar}}{E_a} m_1 m_2 n_1 n_2\right) +$$
$$+ \frac{(n_1 l_2 + l_1 n_2)^2}{3E_t}(1 + 5\alpha^2 + 6\mu_{tr}) + \frac{(l_1 m_2 + l_2 m_1)^2}{G_{ta}} + \frac{(m_1 n_2 + m_2 n_1)^2}{G_{ar}} \tag{51}$$

the same, with the use of (37):

$$\frac{1}{G_{x'y'}} = 4\left(\frac{n_1^2 n_2^2}{E_r} + \frac{l_1^2 l_2^2}{E_t} + \frac{m_1^2 m_2^2}{E_a}\right) - 8\left(\frac{\mu_{rt}}{E_r} n_1 n_2 l_1 l_2 + \frac{\mu_{ta}}{E_t} l_1 l_2 m_1 m_2 + \frac{\mu_{ar}}{E_a} m_1 m_2 n_1 n_2\right) +$$
$$+ \frac{(n_1 l_2 + l_1 n_2)^2}{E_t}(3 - \alpha^2 + 2\mu_{tr}) + \frac{(l_1 m_2 + l_2 m_1)^2}{G_{ta}} + \frac{(m_1 n_2 + m_2 n_1)^2}{G_{ar}} \tag{52}$$

Thus, upon transition from radial to tangential direction, the elastic modulus changes from the value E_r to E_t, taking at $\theta = 45$ the value E_t, subsequently passing through the minimum E_{min}.

Such rather simple method to determine the value of the elastic modulus $E_{xy}^{(45)}$ opens wide possibilities for application of equations obtained by Ye.K. Ashkenazi, A.N. Mitinsky, S. G. Lekhnitsky, with the purpose to calculate other elastic constants.

Excluding the Poisson's ratio from these equations, we obtain the following dependencies:

$$E_{x'} = E_t \Bigg/ \left[\alpha^2 \cos^4\theta + \sin^4\theta + \left(\frac{4E_t}{E_{xy}^{(45)}} - \alpha^2 - 1\right)\cos^2\theta \sin^2\theta\right] \tag{53}$$

$$\frac{1}{G_{x'y'}} = \frac{\cos^2 2\theta}{G_{rt}} + \frac{\sin^2 2\theta}{G_{xy}^{(45)}} \tag{54}$$

The elastic modulus $E_{xy}^{(45)}$ can also be calculated using equations (53), (45).

Equating the terms in round brackets in equations (45) and (53), we obtain the following:

$$\frac{1}{G_{rt}} - \frac{2\mu_{rt}}{E_r} = \frac{4}{E_{xy}^{(45)}} - \frac{1}{E_r} - \frac{1}{E_t} \tag{55}$$

where $\dfrac{1}{G_{rt}} - \dfrac{2\mu_{rt}}{E_r} = \dfrac{B}{E_t}$ or $B = \dfrac{E_t}{G_{rt}} - 2\alpha^2\mu_{rt}$

The last correlation interconnects elastic constants in the plane XY for a cylindrically anisotropic body. Upon solving differential equation (8) in polynomials, this correlation takes the value satisfying the differential equation:

$$B = 3 - \alpha^2 \tag{56}$$

Then, $\dfrac{3 - \alpha^2}{E_t} = \dfrac{4}{E_{xy}^{(45)}} - \dfrac{1}{E_r} - \dfrac{1}{E_t}$

After rearrangements, the following is obtained:

$$E_{xy}^{(45)} = E_t \tag{57}$$

Equation (52) for the elastic modulus will have the following form:

$$\frac{1}{E_{x'}} = \frac{\cos^4\theta}{E_r} + \frac{\sin^4\theta}{E_t} + \frac{3 - \alpha^2}{E_t}\cos^2\theta\sin^2\theta \tag{58}$$

– for the Poisson's ratio:

$$\mu_{x'y'} = -E_{x'}\left[\frac{2(\alpha^2 - 1)}{E_t}\sin^2\theta\cos^2\theta - \frac{\mu_{rt}}{E_r}\right] \tag{59}$$

The first two extreme values (at $\theta = 0°$ and $\theta = \pi/2$) correspond to the principal anisotropy planes. The third value can be found by equating the multiplier in square brackets to zero:

$$-2\alpha^2\cos^2\theta + 2\sin^2\theta + (3 - \alpha^2)(\cos^2\theta - \sin^2\theta) = 0$$

After rearrangement of the last equation, the following is obtained:

$$3\cos^2\theta - \sin^2\theta = 0 \tag{60}$$

wherefrom the value of angle θ: $\theta = \operatorname{arctg}\sqrt{3} = 60°$

It should be noted that the abscissa of extremum point does not depend from the type of material and the angle θ equals 60°.

The extreme value of the elastic modulus corresponding to this angle is as follows:

$$E_{x'} = E_{min} = 8E_t \Big/ (9 - \alpha^2) \tag{61}$$

As per the calculation results, it can be concluded that the elastic modulus reaches its minimum value when the slope angle of the growth ring relative to the board face (as an example, wood is taken) equals 30°.

It is interesting that, at $\theta = 45°$, the transverse elastic modulus has the value equal to Et.

With account for B=3−α², the shear modulus can be calculated using the equation obtained after rearrangement of (54):

$$\frac{1}{G_{x'y'}} = \frac{8(\alpha^2 - 1)}{E_t}\sin^2\theta\cos^2\theta + \frac{1}{G_{rt}} \tag{62}$$

Considering that B=3−α², and, on the other side, $B = \dfrac{E_t}{G_r} - \dfrac{2\mu_t E_t}{E_r}$ we will obtain the following:

$$3 - \alpha^2 = \frac{E_t}{G_{rt}} - \frac{2\mu_{rt} E_t}{E_r} \text{ or } G_{rt} = \frac{E_t}{3 - \alpha^2 + 2\mu_{tr}} \tag{63}$$

Considering (63), equation (62) will take the following form:

$$\frac{1}{G_{x'y'}} = \frac{8(\alpha^2 - 1)}{E_t}\sin^2\theta\cos^2\theta + \frac{3 - \alpha^2 + 2\mu_{tr}}{E_t} \tag{64}$$

For the shear modulus upon rotation of axes, we will obtain the following equation:

$$G_{x'y'} = \frac{E_t}{2(\alpha^2 - 1)\mathrm{Sin}^2 2\theta + 3 - \alpha^2 + 2\mu_{tr}} \quad (65)$$

Let us analyze the obtained function (65) to find the extreme value, i.e. $\frac{d}{d\theta}\left(G_{x'y'}\right) = 0$, and then we will get the following equation:

$$4(\alpha^2 - 1)E_t \mathrm{Sin}4\theta = 0 \quad (66)$$

whence it follows that its left part becomes zero in case when Sin4θ is equal to zero, i.e. at θ=0, θ=45° and θ=90°.

At θ=0 and θ=90° we will get the same values: $G_{x'y'} = G_t$.

At θ = 45° the shear modulus will have the maximum value:

$$G_{x'y'}^{(45)} = G_{45} = \frac{E_t}{\alpha^2 + 1 + 2\mu_{tr}} \quad (67)$$

After rearrangements, equation (67) will coincide with equation (31) as in (Ashkenazi, Ganov, 1981; Ashkenazi, 1978, Lekhnitsky, 1957).

To calculate the Poisson's ratio $\mu_{x'y'}$, let us use equation (59) and substitute the following in it:

$$\frac{1}{G_{xy}} - \frac{2\mu_{xy}}{E_x} = \frac{1}{G_{rt}} - \frac{2\mu_{rt}}{E_r} = \frac{3 - \alpha^2}{E_t} \quad (68)$$

$$\mu_{x'y'} = \frac{2(1 - \alpha^2)\mathrm{Sin}^2\theta\mathrm{Cos}^2\theta - \frac{3 - \alpha^2}{2} + \frac{E_t}{2G_{rt}}}{\alpha^2\mathrm{Cos}^4\theta + (3 - \alpha^2)\mathrm{Sin}^2\theta\mathrm{Cos}^2\theta + \mathrm{Sin}^4\theta} \quad (69)$$

– for the angle θ=45°:

$$\mu_{x'y'}^{(45)} = \frac{E_t}{2G_{rt}} - 1 \quad (70)$$

Theoretically, at some values of E_t and G_{rt}, the positive value of the Poisson's ratio $\mu_{x'y'}^{(45)}$ can be obtained from (69), which was observed by Ye.K. Ashkenazi in experiments.

Let us demonstrate the process of calculating the Poisson's ratio $\mu_{x'y'}$ using the existing experimental data E_t, α^2 (Ashkenazi, Ganov, 1981) for natural composites with an example.

Example 1

It is required to calculate the Poisson's ratios for pine at $E_t = 582MPa$, $\alpha^2 = 0.5178$.

The calculated value G_{rt} as per equation (53) is as follows:

$$G_{rt} = 187.6MPa \quad .$$

Then:

θ=0°; $\mu_{x'y'} = \dfrac{-3 + 0.5178 + 582/187.6}{2 \cdot 0.5178} = 0.5980$

θ=90°; $\mu_{x'y'} = \dfrac{-3 + 0.5178 + 582/187.6}{2} = 0.31$

θ=45°;

$$\mu_{x'y'}^{(45)} = \frac{2(1 - 0.5178) \cdot 0,25 - \dfrac{3 - 0.5178}{2} + \dfrac{582}{2 \cdot 187.6}}{0.5178 \cdot 0.25 + (3 - 0.5178) \cdot 0.25 + 0.25} = 0.553$$

As per the invariant relation $E_t / E_r = \mu_{tr} / \mu_{rt}$, which is known in the task involving wood ($\alpha^2 = 0.5178$), if we take one of the Poisson's ratios according to the experimental data (Ashkenazi, Ganov, 1981), e.g. μ_{tr} = 0.31, then μ_{rt} = 0.5987 (the empirical value as per (Ashkenazi, Ganov, 1981): μ_{rt} = 0.64) will be obtained. On the contrary, at μ_{rt} = 0.64, the value μ_{rt} = 0.33 will be obtained, which is quite close to the empirical value.

Example 2

It is required to calculate the Poisson's ratios for spruce at E_t = 400 MPa

$G_{rt} = 136.5MPa$

$\alpha^2 = 0.5706$

$$\mu_{x'y'} = \mu_t = -E_x\left[\left(\frac{\alpha^2}{E_t} + \frac{1}{E_t} - \frac{3 - \alpha^2}{E_t}\right)\mathrm{Sin}^2\theta\mathrm{Cos}^2\theta + \frac{3 - \alpha^2}{2E_t} - \frac{1}{2G_t}\right] =$$

$$= \frac{-E_t}{\alpha^2\mathrm{Cos}^4\theta + \mathrm{Sin}^4\theta + (3 - \alpha^2)\mathrm{Cos}^2\theta\mathrm{Sin}^2\theta}\cdot\left[\frac{2(\alpha^2 - 1)\mathrm{Sin}^2\theta\mathrm{Cos}^2\theta}{E_t} + \frac{3 - \alpha^2}{2E_t} - \frac{1}{2G_t}\right] =$$

$$= -\frac{3 - \alpha^2}{2\alpha^2} + \frac{E_t}{2G_t\alpha^2} = \frac{3 - 0.5706}{2 \cdot 0.5706} + \frac{400}{2 \cdot 136.5 \cdot 0.5706} = 0.439$$

$\mu_{rt} = 0.439$ The table value of $\mu_{rt} = 0.42$

$\mu_{tr} = 0.439 \cdot \alpha^2 = 0.439 \cdot 0.5706 = 0.2505$

The table value of $\mu_{rt} = 0.25$.

Correlations based on the requirement for the positive value of elastic potential are as follows:

$$\mu_a < \sqrt{E_a / E_r} \; ; \quad \mu_{ta} < \sqrt{E_t / E_a} \; ; \quad \mu_{rt} < \sqrt{E_r / E_t} \quad (71)$$

Fulfillment of the following correlation for an orthotropic body is checked (Ashkenazi, Ganov, 1981):

$$\frac{2}{E_r} + \frac{2}{E_t} + \frac{1}{G_{rt}} = \frac{4}{E_{xy}^{(45)}} + \frac{1}{G_{45}}$$

$$\frac{2\alpha^2}{E_t} + \frac{2}{E_t} + \frac{3 - \alpha^2 + 2\mu_{tr}}{E_t} = \frac{4}{E_t} + \frac{\alpha^2 + 1 + 2\mu_{tr}}{E_t}$$

$$\frac{2\alpha^2 + 2 + 3 - \alpha^2 + 2\mu_{tr}}{E_t} = \frac{5 + \alpha^2 + 2\mu_{tr}}{E_t}$$

The correlation is observed, the left and right parts are identically equal.

The same correlation is observed for pine wood:

$$\frac{2}{1124} + \frac{2}{582} + \frac{1}{187.6} = \frac{4}{582} + \frac{1}{272.2}$$

The value of the directional cosine determining the position of axis X', relative to which the function of the elastic modulus $E_{x'}$ takes the extreme value (in the XY

Table 2. Elastic constants for several wood species.

Wood specie	E_t, MPa	G_{rt}, MPa	$\alpha^2 = E_t/E_r$	Poisson's ratio as per equation (69) at the following slope angles of the growth ring						
				$\theta = 0°$	15°	30°	45°	60°	75°	90°
Pine	582	187.6	0.5178	0.6 0.64*	0.6068	0.59925	0.553	0.463	0.3646	0.31 0.31*
Spruce	400	136.5 347*	0.5706	0.44 0.42*	0.4658	0.4905	0.4652	0.3905	0.2962	0.25 0.25*
Beech	1,160	361.1 467*	0.5077	0.71 0.75*	0.7	0.668	0.596	0.513	0.4098	0.36 0.36*
Oak	985	312.8 403*	0.4508	0.665 0.64*	0.6689	0.6412	0.575	0.4766	0.36	0.30 0.30*
Ash	818	256.6 284*	0.5322	0.6765 0.71*	0.6728	0.6493	0.594	0.50586	0.4074	0.36 0.36*
Fir	490	154.1 150*	0.5213	0.672 0.60*	0.6692	0.646	0.59	0.5	0.3993	0.35 0.35*
Maple	890	275.9 287*	0.5742	0.6966 0.82*	0.691	0.6660	0.613	0.531	0.442	0.4 0.40*

Note: * – experimental values (Ashkenazi, Ganov, 1981).

Table 3. Elasticity characteristics of filament-wound fiberglass as per the data presented in some publications (Glukhikh, 2008) and as per the results of author's calculations (given in brackets).

Elasticity characteristics	Filler			
	Strand 19 of VM-1 fiber	VM-1 fiber	Strand 19 of VM-1 fiber	VM-1 fiber
	Ratio of fibers			
	$n = \infty$	$n = 5$	$n = 2$	$n = 1$
E_a, MPa	5.7	4.76	3.68	3.09
E_r, MPa	1.4	2.07	2.68	2.74
E_t, MPa	1.4	1.45	1.10	1.05
E_{ar}, MPa	1.58 (1.4)	1.59 (2.07)	1.56 (2.68)	1.28 (2.74)
E_{rt}, MPa	1.4 (1.4)	1.26 (1.45)	1.19 (1.10)	1.07 (1.05)
E_{ta}, MPa	1.58 (1.4)	1.45 (1.45)	1.24 (1.10)	1.07 (1.05)
B''	2.3	3.77	5.15	6.7
G_{ar}, MPa	0.575 (0.484)	0.531 (0.768)	0.505 (1.105)	0.396 (1.174)
B	2	2.89	3.02	2.526
G_{rt}, MPa	0.5 (0.5)	0.436 (0.526)	0.414 (0.373)	0.369 (0.358)
B'	2.3	2.7	2.25	2.62
G_{ta}, MPa	0.575 (0.484)	0.501 (0.500)	0.447 (0.374)	0.366 (0.356)
μ_{ar}	0.277	0.149	0.105	0.123
μ_{ra}	0.068	0.065	0.077	0.110
μ_{rt}	0.4	0.325	0.431	0.417
μ_{tr}	0.4	0.227	0.177	0.160
μ_{ta}	0.068	0.099	0.105	0.151
μ_{at}	0.277	0.325	0.353	0.443

plane at $l_1 = 0$), can be found using the following equation (Ashkenazi, 1978):

$$l_1 = \pm \sqrt{\frac{\dfrac{3}{E_t} + \dfrac{1}{E_r} - \dfrac{4}{E_{xy}^{(45)}}}{\dfrac{4}{E_t} + \dfrac{4}{E_r} - \dfrac{8}{E_{xy}^{(45)}}}} = \pm \sqrt{\frac{\dfrac{3}{E_t} + \dfrac{\alpha^2}{E_t} - \dfrac{4}{E_t}}{\dfrac{4}{E_t} + \dfrac{4\alpha^2}{E_t} - \dfrac{8}{E_t}}} = \pm \frac{1}{2}$$

i.e. $\mathrm{Cos}(x, x') = \pm \dfrac{1}{2}$

Thus, the angle between axes X and X' is equal to 60°. The same result was obtained above. The second directional cosine:

$$m_1 = \pm \sqrt{1 - l_1^2} = \pm \sqrt{1 - \frac{1}{4}} = \pm \frac{\sqrt{3}}{2},$$

which corresponds to the angle of 30°.

For equal-reinforced composites ($\alpha^2 = 1$), this angle is equal to 45°.

The available standards stipulate for experimental determination of 18 elasticity characteristics $\left(3E_i, 3G_{ik}, 3\mu_{ik}, 3E_{ik}^{(45)}, 3\mu_{ik}^{(45)}\right)$.

According to the results, the shear moduli are determined using the following equation:

$$G_{ik} = \frac{E_{ik}^{(45)}}{2\left(1 + \mu_{ik}^{(45)}\right)}$$

As the correlation ($B = 3 - \alpha^2$) is established between elastic constants, there is no need in experimental determination of $E_{ik}^{(45)}$, $\mu_{ik}^{(45)}$. To determine elastic constants, it is sufficient to know their values relative to principal anisotropy axes ($3E_i$; $3\mu_{ik}$; $3\mu_{ki}$).

Using the equations obtained above, it is possible to determine values of elastic constants relative to any axes position.

If the ratio between elastic constants corresponds to dependency (34, a) for some composites, then equations for the elastic modulus, Poisson's ratio, and shear modulus will be as follows:

$$\frac{1}{E_{x'}} = \frac{\mathrm{Cos}^4\theta}{E_r} + \frac{1 + 5\alpha^2}{3E_t}\mathrm{Sin}^2\theta\mathrm{Cos}^2\theta + \frac{\mathrm{Sin}^4\theta}{E_t} \tag{72}$$

$$\frac{1}{E_{y'}} = \frac{\mathrm{Sin}^4\theta}{E_r} + \frac{1 + 5\alpha^2}{3E_t}\mathrm{Sin}^2\theta\mathrm{Cos}^2\theta + \frac{\mathrm{Cos}^4\theta}{E_t} \tag{73}$$

$$\frac{1}{G_{x'y'}} = \frac{8\left(1 - \alpha^2\right)}{3E_t}\mathrm{Sin}^2\theta\mathrm{Cos}^2\theta + \frac{1}{G_{rt}} \tag{74}$$

$$\mu_{x'y'} = -E_{x'}\left[\frac{2\left(1 - \alpha^2\right)}{3E_t}\mathrm{Sin}^2\theta\mathrm{Cos}^2\theta - \frac{\mu_{rt}}{E_r}\right] \tag{75}$$

$$E_{xy}^{(45)} = \frac{3E_t}{1 + 2\alpha^2} \tag{76}$$

Upon an analysis of function (72) to find the extreme value, the following equation is obtained:

$$\mathrm{Cos}^2\theta + 5\mathrm{Sin}^2\theta = 0,$$

whence it follows that the elastic modulus $E_{x'}$ does not take the third extreme value upon rotation of axes. At $B < 2$, composites have only two main modulus values: E_r and E_t.

Analyzing shear modulus function (74) at rotation of axes in the plane of cross-section to find the extreme value, similar extreme values (as at $B = 3 - \alpha^2$) are obtained. At other values of the angle θ, shear moduli differ.

Based on equation (75), it is possible to obtain the value of the Poisson's ratio at $\theta = 45°$:

$$\mu_{x'y'}^{(45)} = \frac{3E_t}{2\left(1 + 2\alpha^2\right)G_{rt}} - 1 \tag{77}$$

The Poisson's ratio can be positive if the following correlation is observed:

$$\frac{E_t}{2G_{rt}} < \frac{1 + 2\alpha^2}{3} \tag{78}$$

Comparison of calculated values of elastic constants using the obtained equations with the experimental data for a cylindrically anisotropic body through the example of fiberglass materials (Table 3) allows checking the original assumptions underlying the conclusion on their applicability to the examined material. At the B value within the range from 2 to 3, calculated values of elasticity characteristics are quite close to the experimental ones. At values exceeding 3, noticeable deviation of the calculated shear modulus G_{ar} from the experimental value is observed. This is due to the fact that at values exceeding 3, the parameter B does not satisfy differential equation (1). The B value can be affected by inaccuracy in determination of μ_{ra}, G_{ar}, and imperfection of experiment methods.

References

Ashkenazi, Ye.K. (1978). *Anizotropiya drevesiny i drevecnyh materialov [Anisotropy of wood and wood materials]*. Moscow: Lesnaya Promyshlennost (Forest Industry). (in Russian)

Ashkenazi, Ye.K., Ganov, V.V. (1981). *Anizotropiya konstrukcionnyh materialov [Anisotropy of structural materials]*. Moscow: Lesnaya Promyshlennost (Forest Industry).(in Russian)

Glukhikh, V.N. (1997). *K voprosu o reshenii v polinomah ploskoj zadachi teorii uprugosti dlya pryamougol'noj cilindricheski anizotropnoj polosy [Concerning the solution of the plane problem of the elasticity theory for a rectangular cylindrically anisotropic strip (in polynomials)]*. Saint Petersburg: Saint Petersburg State Forest Technical University. (in Russian)

Glukhikh, V.N. (1998). Ploskaya zadacha teorii uprugosti dlya cilindricheski anizotropnogo tela v dekartovyh koordinatah [Plane problem of the elasticity theory for a cylindrically anisotropic body in Cartesian coordinates]. *News of the Saint Petersburg State Forest Technical Academy*, 6 (164), pp. 141–145. (in Russian)

Glukhikh, V.N. (2001). *Primenenie polinomov k resheniyu zadach dlya cilindricheski anizotropnogo tela [Application of polynomials in the solution of problems for a cylindrically anisotropic body]*. Saint Petersburg: Saint Petersburg State Forest Technical University. (in Russian)

Glukhikh, V.N. (2007). Uprugie postoyannye cilindricheski anizotropnogo tela [Elastic constants of a cylindrically anisotropic body]. *Journal International Academy of Refrigeration*, 2. (in Russian)

Glukhikh, V.N. (2008). Svyaz' mezhdu uprugimi postoyannymi cilindricheski anizotropnogo tela [Relations between elastic constants of a cylindrically anisotropic body]. *Journal International Academy of Refrigeration*, 1. (in Russian)

Glukhikh, V.N. (2010). Differential equations for a cylindrically anisotropic body considering obtained correlations between independent elastic constants. In: *Proceedings of the 4th International Eurasian Symposium*. Yekaterinburg: Ural State Forest Engineering University, pp. 48–54. (in Russian)

Grigorovich, V.K. (1952). O naivygodnejshem napravlenii volokon v izdeliyah iz anizotropnyh materialov [Concerning the most favorable direction of fibers in products made of anisotropic materials]. *Proceedings of the USSR Academy of Sciences*, 86 (4), pp. 152–160. (in Russian)

Kuffner, M. (1978). Elastizitatsmodul und Zugfestigkeit von Holz verschiedenen Rohdichte in Abhangigkeit vom Feuchtigkeitgehalt [Modulus of elasticity and breaking strength factor of wood of different true specific density, depending on the moisture content]. *Wood as a Raw Material and Goods*, 11, pp. 435–440. (in German)

Kurdyumov, N. (1946). Reshenie v polinomah ploskoj zadachi teorii uprugosti [Solution of the plane problem of the elasticity theory (in polynomials)]. *PMM*, XI. (in Russian)

Lekhnitsky, S.G. (1957). *Anizotropnye plastinki [Anisotropic plates]*. Moscow: Gostekhizdat. (in Russian)

Lekhnitsky, S.G. (1977). *Teoriya uprugosti anizotropnogo tela [Theory of anisotropic body elasticity]*. Moscow. (in Russian)

Mitinsky, A.N. (1948). Uprugie postoyannye drevesiny kak ortotropnogo materiala [Elastic constants of wood as an orthotropic material]. *Proceedings of the Forest Academy*, 63, pp. 22–54. (in Russian)

Mitinsky, A.N. (1949). Torsion and shear moduli of wood as an anisotropic material. *Proceedings of the Forest Academy*, 65, pp. 49–57. (in Russian)

Rabinovich, A.L. (1946). *Ob uprugih postoyannyh i prochnosti anizotropnyh materialov [Concerning elastic constants and strength of anisotropic materials]*. Moscow: Buro novoi tekhniki. (in Russian)

Rosato, D.V., Grove, C.S. (1969). *Namotka steklonit'yu [Filament winding]*. Translated from English. Moscow: Mashinostroyeniye. (in Russian)

Ylinen, A. (1952). Uber die mechanische schaftformtheorie der Baume [On the mechanic theory of the stem form of trees]. *Scientific Researches*, 6. (in German)

COMPARATIVE ANALYSIS OF ENERGY CONSUMPTION BY MODERN CARS AND FUTURE QUANTOMOBILES

Jurij Kotikov

Saint Petersburg State University of Architecture and Civil Engineering
Vtoraja Krasnoarmejskaja ul., 4, St. Petersburg, 190005, Russia

cotikov@mail.ru

Abstract

Features of the theory of Superunification, used in formation of quantum engine (QE) concepts, are briefly described in the article. Schemes of thrust formation in QEs are considered. A concept of a quantum car (quantomobile) as a vehicle with a quantum engine, preserving supporting idle wheels, is introduced.

Complete removal of idle wheels in a quantomobile leads to a concept of a flying car. Analytical comparison of Kamaz-4326 truck horizontal thrust and energy consumption with indicators of hypothetical quantomobile and flying car (based on such car) concepts is conducted.

Keywords

Car, quantum engine, quantomobile, flying car, quantum thrust, energy consumption.

Introduction

Efforts of scientists in search of a new paradigm of energy supply for humanity over the past decades (Einstein (1963), Tesla (2009), Dirac (Dirac, 1927, 1930; Sanyuk, 2009), Parker (1991), Davies (1985), Puthoff (2010), Veinik (1991), Petrov (2015), Shawyer (2006), McCulloch (2014), Fetta (2014), Tajmar (2018), and others) were crowned with unveiling of the structure and energy density of the physical vacuum, super-strong electromagnetic interaction (SEI). An insight into the above-mentioned subjects is provided by the t*heory of Superunification* suggested by Leonov V.S. (Leonov, 2002, 2010a, 2010b, 2018).

The ability to draw energy from the global physical vacuum will result in a new technological paradigm involving the transport sector as well. Quantum engines will replace internal combustion and jet engines; the existing propulsion devices of vehicles will improve.

In his publications (Kotikov, 2018a, 2018b), the author of the article considered basic provisions of the theory of Superunification, suggested by Leonov, in general terms, described aspects of QE development, predicted some features of cars with QEs (quantomobiles), and reviewed stages of research and practical implementation of QEs and quantomobiles.

The purpose of the article is to create a methodology to compare energy consumption indicators and perform a comparative quantitative assessment of energy consumption by modern cars and future (hypothetical) quantomobiles.

Ideas of the theory of Superunification promoting QE creation

In the author's opinion, fundamental theoretical developments of Leonov V.S. and his theory of Superunification (Leonov, 2010a) referring to the process of such quantization of Einstein's space-time, which allowed uniting electromagnetic, gravitational, nuclear and electroweak forces into one field entity (Superforce (Davies, 1985)) (at the time, Einstein made similar attempts but failed due to objective reasons — the lack of
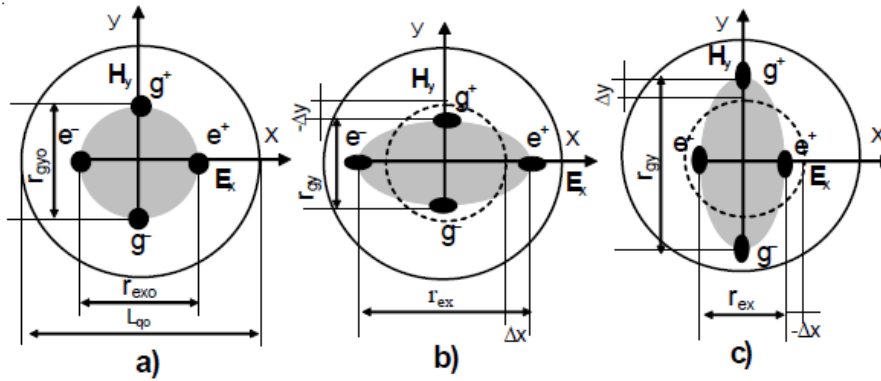
Figure 1. Electromagnetic polarization of the quanton upon the passage of an electromagnetic wave: (a) equilibrium (zero) state of the quanton; (b), (c) perturbed polarized state of the quanton (Leonov, 2010a).

developments in physics), are the most successful works in the field of investigating the structure of the physical vacuum. Leonov borrowed the concept of a quark (an elementary component of the primordial matter) from the Standard Model and simplified it by removing quarks with fractional electric charges. Four quarks made up the quanton structure. The quanton (the only universal four-dimensional particle) became the carrier of time and space.

Quantization is an energy process. The global physical vacuum — the quantized space-time (QST) (including real insertions) — is densely filled with quantons that are mobile within their small neighborhood.

A quanton is a quadrupole consisting of two dipoles — an electric one and a magnetic one — orthogonally placed inside it. Generation or conduction of an electromagnetic wave is carried out by changing the axial distances (arms) between the charges (quarks) of each of the dipoles (see Figure 1) (Leonov, 2010a).

Figure 2. Modeling of elementary particles in the form of regions of spherically deformed QST: RS — gravitational medium interface; ρ_1 — tension field (light-colored), ρ_2 — compression field (dark-colored) (Leonov, 2010a).

Gravitational transformations of the unified field of QST represent spherical Einstein's curvatures of QST due to displacement of quantons in their small neighborhood (their concentration around some short-time pole within a fragment upon simultaneous rarefaction of the fragment periphery) (see Figure 2) (Leonov, 2010a).

The ensemble of quantons in spherically deformed QST ensures ponderomotive (force) interaction between electromagnetism and gravity, which was confirmed experimentally. Actual anti-gravity effects were found (Leonov, 2010a).

If we introduce a perturbing electric charge into QST, quantons will be attracted to that electric charge. QST, being an elastic medium, tends to compress near the perturbing charge. However, this is possible only due to tension in a distance from the central charge. A process of spherical deformation of the quantized medium occurs (Leonov, 2010a).

The theory of Superunification considers mass movement as wave transfer of QST spherical deformation.

QST can also be characterized as a scalar field with the distribution of the medium quantum density ρ (x, y, z). The medium quantum density represents the concentration of quantons per unit of volume. Then the emergence of an elementary particle as a result of compression/tension of the medium from the perspective of vector analysis is the divergence of the gradient of the quantum medium density (Leonov, 2010a).

An equation characterizing an elementary particle in QST is as follows (Leonov, 2010a):

$$\mathrm{div}\left(\mathrm{grad}\rho\right) = k_o \rho_m \tag{1}$$

where k_o — proportionality coefficient;
ρ_m — matter density, kg/m^3.

Let us note that *div* is an operator, projecting the vector field to the scalar field. The gradρ gradient which is a part of (1) represents the medium deformation vector **D** when the scalar field ρ (x, y, z) is used to create a vector field upon deformation, characterizing gravity emergence (Leonov, 2010a):

$$\mathbf{D} = \mathrm{grad}\rho \tag{2}$$

Equation (2) shows that deformed QST, being a carrier of SEI, is the basis of gravity (Figure 2). Gravity is basically electromagnetic in its nature.

Leonov expresses the force of gravitation F_m through the deformation vector **D** of QST (Leonov, 2010a):

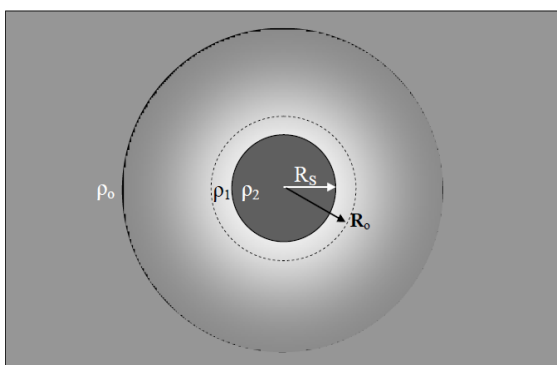$$\mathbf{F}_m = \frac{C_0^2}{\rho_0} m \cdot \mathrm{grad}\rho = \frac{C_0^2}{\rho_0} m \cdot \mathbf{D} \tag{3}$$

where C_0^2 is the maximum gravitational potential of the unperturbed QST;

ρ_0 is QST density.

The deformation vector **D** in (2) and (3) is an analogue of the gravitational field strength vector **a** (where **a** is free-fall acceleration) (Leonov, 2010a):

$$\mathbf{a} = \frac{C_0^2}{\rho_0}\mathbf{D} \qquad (4)$$

According to the theory of Superunification, gravity cannot emerge outside QST, and it is based on the real deformation of QST. A gravitational pit forms around any object having a mass. The considered proof mass *m* affected by the gravitational force $\boldsymbol{F}_m$ rolls down into the gravitational pit to the perturbing mass *M*, implementing their mutual gravitational attraction (Leonov, 2010a).

Concepts of thrust formation in quantum engines

The technology of creating the force of artificial gravitation has already been implemented by Leonov V.S. in a number of trial designs of quantum (field) engines that generate a thrust impulse due to the interaction of QE operating elements with QST without the ejection of the reactive mass (Leonov, 2002, 2010a, 2010b, 2018).

In the field theory, the direction and magnitude of the force vector **F** (being determined by the spatial gradient (grad) of energy W) are oriented towards a decrease in energy (Leonov, 2010a):

$$\mathbf{F} = \text{gradW} \qquad (5)$$

Differentials in energy levels in space determined by the energy gradient (5) lead to the emergence of a force, to force interaction.

If the global energy field W is a scalar field, then the gradient (5) describes a vector force field having the direction and magnitude of the fastest change in energy W in partial derivatives and can be written with the use of the Hamiltonian operator (Heaviside, 1893; Leonov, 2018):

$$\text{gradW} = \nabla W = \frac{\partial W}{\partial x}\mathbf{i} + \frac{\partial W}{\partial y}\mathbf{j} + \frac{\partial W}{\partial z}\mathbf{k} \qquad (6)$$

where **i, j, k** are unit vectors along the x, y, z axes, respectively.

If we need forces to emerge, it is necessary to create energy level differentials in the energy field, when W ≠ const. The force modulus (6) is determined by the following equation (Heaviside, 1893; Leonov, 2018):

$$\left|\text{gradW}^2\right| = \sqrt{\left(\frac{\partial W}{\partial x}\right)^2 + \left(\frac{\partial W}{\partial y}\right)^2 + \left(\frac{\partial W}{\partial z}\right)^2} \qquad (7)$$

The direction of the unit gradient vector (force direction) **n** is determined by the ratio of the function (6) to its modulus (7) (Heaviside, 1893; Leonov, 2018):

$$\mathbf{n} = \frac{\text{gradW}}{\left|\text{gradW}^2\right|} = \frac{\dfrac{\partial W}{\partial x}\mathbf{i} + \dfrac{\partial W}{\partial y}\mathbf{j} + \dfrac{\partial W}{\partial z}\mathbf{k}}{\sqrt{\left(\dfrac{\partial W}{\partial x}\right)^2 + \left(\dfrac{\partial W}{\partial y}\right)^2 + \left(\dfrac{\partial W}{\partial z}\right)^2}} \qquad (8)$$

Equations (5)...(8) are valid for calculations of the force when energy diffuses in space unevenly and energy differentials are observed, and when the function of energy distribution in space W = f (x, y, z) is known (Leonov, 2018).

The theory of Superunification provides the scientific basis for the creation of an artificial thrust (changing the direction of the force vector **n**).

In order to create an artificial thrust, it is necessary to create an energy gradient inside the proof mass (body) (QE operating unit) due to the redistribution of the medium quantum density (Leonov, 2018).

For instance, in 2002, in his patent, Leonov created an energy gradient (Leonov, 2002) due to the use of the conic shape of the operating unit and the effect of an external electromagnetic field with crossing electric and magnetic fields on the conical operating unit. So far, he has implemented a dozen of methods to create an artificial thrust in various designs of quantum engines: both with rotating and non-rotating operating elements (Leonov, 2018). Formation of directional wave motion of the QST curvature front, according to Figure 1 (Leonov, 2010a), represents a common feature for all methods and devices.

For instance, according to a design suggested by Shawyer (2006), the thrust **F** is created due to the interaction of the gradient SHF field with QST. The SHF field creates a gradient of the medium quantum density and energy inside the conical resonator (Figure 3) (Branderburg, 2017).

Both the magnetron, and conical resonator represent an integral part of QST, freely penetrating it. Under the influence of the gradient field, the effect of the "drawing-in" of QST quantons in the diffuser of the conical resonator is observed. Since QST is stationary, the "drawing-in" effect manifests as the movement of the quantum engine in space under the influence of the thrust **F** (Figure 3). It turns out that the quantum engine, creating the thrust
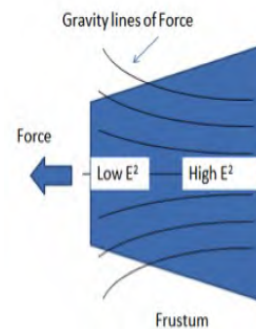

Figure 3. EmDrive microwave quantum engine with a conical resonator (Branderburg, 2017).

F, kind of moves in QST (in the front), pushing off this space as from an elastic quantized medium (in the back) (Leonov, 2018).

The thrust **F** direction in Figure 3 is conventional. It can vary and even become reverse, depending on the design of the resonator, placement of channels leading from the magnetron to the resonator, characteristics of the SHF field (McCulloch, 2014).

Let us call the force **F** the "traction force" (denoting it as F_T) (in terms of its application to vehicle's structural elements) as well as the "thrust force" (in terms of the field response to its perturbations in the resonator (the term is borrowed from rocketry).

In case the resonator is rigidly mounted onto the vehicle's body and there are no intermediate force transducers, both things will mean the same. However, if there are intermediate transducers (dampers, reduction gears, etc.), those forces may differ.

It should also be noted that the force (vector) can be decomposed into unit vectors:

$$F_T = F_{T_X} + F_{T_Y} + F_{T_Z} \tag{9}$$

The scalar form of this equation is as follows:

$$F_T = \sqrt{F_{Tx}^2 + F_{Ty}^2 + F_{Tz}^2} \tag{10}$$

We will consider the derivations presented above to be necessary and sufficient to create a method for comparative analysis of power drives of the existing and hypothetical vehicles.

Method for comparative power and energy analysis of vehicles with internal combustion engines (ICEs) and QEs

The purpose of the analysis is to estimate the levels of the required energy consumption in two options of power supply units (with ICEs and QEs) under the same load and driving modes.

We will confine ourselves to the basic driving mode of a long-haul vehicle: driving at a constant speed along a horizontal road section.

Let us start formation of analytical threads from the ICE crankshaft flywheel and QE resonator.

The classical equation of the vehicle's thrust balance for steady motion along a horizontal road section is as follows:

$$P_T = P_f + P_w \tag{11}$$

where P_T — thrust generated by the torque transmitted to the driving wheels, and applied to the frame of the vehicle through the wheel axis (wheel hub);

P_f — rolling resistance;

P_w — wind resistance.

Let us modify equation (11) for the quantomobile by replacing P_T with F_T (see Figure 4), where F_T — thrust generated by the QE and applied to the frame of the quantomobile (at the QE location):

$$F_T = F_f + F_w \tag{12}$$

Before we consider changes for each component of this force balance equation upon the transition from the automobile to the quantomobile, it is useful to compare processes of generating each of the thrust forces: P_T and F_T (the left side of equations). Let us review Figure 4.

Let us note that in contrast to academic courses (where thrust emerges on the axis of the driving wheel), in our case, P_T affects the Vehicle A from the side of the suspension. First, the suspension is an important element of a wheeled mover with energy consumption for vehicle oscillations and power circulation. Second, it serves to ensure that places of such force application are identical for both vehicles under consideration.

The internal combustion engine produces the effective torque output M_e (with the implementation of the effective power N_e at a given speed) which has to undergo a series of transformations in the clutch, gearbox, differentials, transfer gearboxes, final reduction gears, shaft lines, wheels (in their complicated contact with the road) prior to formation of the P_T thrust affecting the frame (body) from the side of the suspension; in each of those links, transformations occur, causing the loss of energy and efficiency coefficient decrease (transmission — η_{tr}, driving wheels — η_{dw}, suspension — η_{susp}), depending on numerous conditions.

The diagram in Figure 4 makes it possible to trace changes in power transmitted from the internal combustion
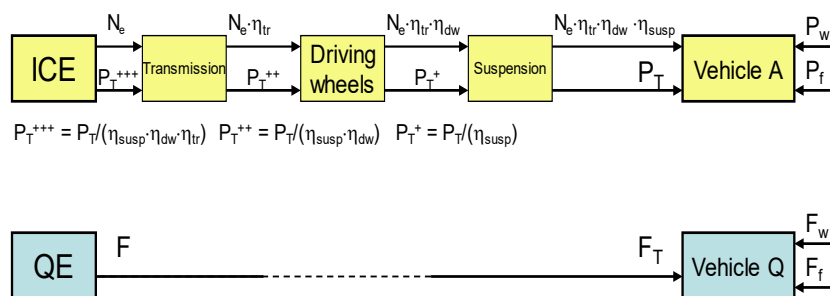

Figure 4. Diagrams of generating thrust forces for the automobile (Vehicle A) and quantomobile (Vehicle Q).

engine through the elements of the power train to the frame of the Vehicle A (in the upper connection layer). The losses are accumulated, which is analytically taken into account in the values of the corresponding efficiency coefficients. In the end, power $N_T = N_e \cdot \eta_{tr} \cdot \eta_{dw} \cdot \eta_{susp}$ is left for the implementation of Vehicle A movement. This power (at a given speed) corresponds to P_T thrust.

P_T force can be brought to the ICE crankshaft, taking into account inverse values of the efficiency coefficient of power components, namely: $P_T+++ = P_T/(\eta_{susp} \cdot \eta_{dw} \cdot \eta_{tr}) = P_T/\eta_{pt}$ where η_{pt} — power train efficiency coefficient.

The values of η_{tr}, η_{dw}, η_{tr} coefficients given in the following quantitative analysis were determined by the author on the basis of numerous models, including his own materials (Kotikov, 2006); the expert-based approach was also applied.

Out of seven wheel-rolling modes of the automobile (Kotikov, 2006) only the driven mode will remain for the wheels of the quantomobile. No power supply is spent on hysteresis losses in tires, work of tire/road external friction forces, interaxial and side-to-side power circulation; ventilation losses are reduced.

During the analysis, we will use the coefficient of rolling resistance of the driving wheel tire f_{tire} (Kotikov, 2006):

$$f_{tire} = P_f / Z = a_t / r_d + M_k(r_d - r_k)/(Zr_d \cdot r_k) = \frac{a_t}{r_d} + \frac{M_k}{Zr_k}\delta_w = f_{force} + f_k \quad (13)$$

where r_d — dynamic radius, r_k — kinematic radius, $f_{force} = a_t / r_d$ is a component of the coefficient f_{tire}, characterizing force losses associated with trail a_t of vertical reaction Z; $f_k = ((M_k/r_k)/Z)\delta_w$ is a component of the coefficient f_{tire}, characterizing kinematic losses associated with wheel slip $\delta_w = (r_d - r_k)/r_d$ leading to the reduction in the driving speed of the vehicle v. Coefficients f_{tire}, f_{force} and f_k are *energy, force* and *kinematic coefficients* of rolling resistance, respectively.

The value $((M_k/r_k)/Z)(r_d - r_k)) = a_k$ determines additional trail of normal reaction Z. Taking into account $(a_t + a_k) = a_{tire}$, the following can be written:

$$f_{tire} = (a_t + a_k) / r_d = ((P_{f\,force} + P_{fk}) / Z = $$
$$= \left(M_{f\,force} + M_{fk}\right) / Zr_k = \left(N_{f\,force} + N_{fk}\right) / Zv \quad (14)$$

where $P_{f\,force}$, P_{fk}, Mf_{force}, M_{fk}, $N_{f\,force}$ and N_{fk} are force and kinematic components of the force P_f, torque M_f and power N_f of wheel rolling resistance.

As the wheel passes from the driving mode to the driven one, wheel slip virtually disappears as the values $(r_d - r_k)$, δ_w, f_k, a_k approach zero. Trail at of vertical reaction Z decreases (let us assume that it decreases by half).

During this analysis, the QE generates thrust F_T (see Figures 3 and 4; $F_T = F$). Throttling and damping functions of the QE control system — to ensure the F_T value sufficient to achieve the thrust balance according to equation (12) — are not considered yet, however, the possibility of introducing such element with account for $F_T \neq F$ is marked by a dotted line in Figure 4.

Taking into account the basic condition for comparing different options: $F_T = P_T$, the energy efficiency of quantomobile movement as compared to that of the automobile can be estimated with the use of the value F_T/P_T+++. In other words, we can estimate how much/less the QE power can be than the ICE power to ensure required steady movement.

Let us represent aerodynamic resistance by the following well-known equation:

$$P_w = k_w \cdot F_{front} \cdot v_w^{\,2} \quad (15)$$

where k_w — wind shape coefficient, N·s²m⁻⁴; F_{front} — frontal area, m²; v_w — vehicle speed in relation to wind, ms⁻¹.

In case of the quantomobile, the following protruding parts are removed from the frontal area profile: drive axles, drive shafts, gearbox housing, muffler, fuel tank.

Aerodynamic characteristics of wheeled vehicles are greatly affected by the air flow pattern under the vehicle body. For quantomobiles and flying cars, we shall take into account reduction of losses under the vehicle body by decreasing the k_w coefficient.

Numerical example

To estimate quantomobile power characteristics compared to those of the modern car, we will consider a numerical example of comparing thrust and energy consumption by the KAMAZ-4326 truck (KAMAZ-master, 2018) (Figure 5) and the hypothetical laboratory

Figure 5. KamAZ-4326 truck (participant of the Dakar Race).

quantomobile based on such truck (in steady movement at a constant speed of 100 km/h (27.8 m/s)).

The load is constant in all design cases; the total mass of the vehicle is reduced due to mass reduction upon the transition from the KAMAZ-4326 truck to the quantomobile, and then to the flying car (which corresponds to purposes of modernization).

Let us consider five design cases:

Table 1. Comparative calculation results.

Indicator	Design cases				
	1. Automobile, ICE, f = 0.01, P_T	2. Automobile, ICE, f = 0.1, P_T	3. Quantomobile, QE, f = 0.01, F_T	4. Quantomobile, QE, f = 0.1, F_T	5. Flying car, QE F_{Tx}
G_{veh}, N	100,000	100,000	88,000	88,000	78,000
F_{front}, m²	7.0	7.0	6.5	6.5	5.5
k_w, N·s²/m⁴	0.6	0.6	0.55	0.55	0.45
η_{tr}	0.85	0.92	-	-	-
η_{dw}	0.9	0.7	-	-	-
η_{susp}	0.97	0.9	-	-	-
η_{pt}	0.74	0.58	-	-	-
P_f, N	1,000	10,000	880	8,800	0
P_w, N	3,240	3,240	2,760	2,760	1,910
P_T (F_T, F_{Tx}), N	4,240	13,240	3,640	11,560	1,910
N_T (N_{Tx}), kW/hp	118/160	368/500	101/137	321/437	53/72
P_e+++ (F_T, F_{Tx}), N	5,730	22,830	3,640	11,560	1,910
N_e (N_{Tx}), kW/hp	159/216.5	634/862	101/137	321/437	53/72

1) KamAZ-4326 truck with ICE YaMZ-7E846.10-07 — on a road with extremely low road resistance f = 0.01;

2) KamAZ-4326 truck with ICE YaMZ-7E846.10-07 — on a road with rather high road resistance f = 0.1;

3) laboratory quantomobile based on KamAZ-4326, with a QE (instead of an ICE with conventionally the same mass), without a standard transmission, with a light-weight suspension with axle beams without a crankcase and with only driven carrying wheels, without fuel tanks and mufflers (the vehicle shall not be loaded up to the initial loading value) — on a road with road resistance f = 0.01;

4) laboratory quantomobile based on KAMAZ-4326, with a QE (instead of an ICE) with the configuration in accordance with item 3 — on a road with road resistance f = 0.1;

5) laboratory flying car based on KamAZ-4326, with a QE (instead of an ICE) with the configuration in accordance with item 3 but without supporting wheels, with a clad floor. Only horizontal directional thrust F_{Tx} (see (9) and (10)) is taken into account.

In each of the five options mentioned above, we shall achieve equal speed rates of the compared vehicles. Under this condition, we determine the difference between the required thrust forces P_T and F_{Tx}, as well as the difference between the values of the required efficient power of the ICE ($N_{e.ICE}$) and QE ($N_{e.QE}$).

Results of the calculations are presented in a summary table. In that table, G_{veh} is the mass of the vehicle with a constant load for all five options: options 1 and 2 — total

mass of 10 tons; options 3 and 4 — mass reduction by 1.2 tons; option 5 — mass reduction by another ton.

Taking into account the fact that energy consumption in steady movement at a constant speed is proportional to the realizable power, it is possible to draw the following conclusions based on the table indicators. Energy consumption by the quantomobile with carrying wheels at a speed of 100 km/h is 1.5–2 times less than that of the KAMAZ-4326 truck (see the N_e (N_{Tx}) line of the table).

Energy consumption of the flying car for the horizontal component of the thrust force $\mathbf{F_{Tx}}$ is three times less than that of the truck under the lowest possible resistance of the horizontal road. The absence of data on energy consumption for vertical suspension of the flying car (component $\mathbf{F_{Tz}}$ of thrust (9)) does not make it possible yet to compare the flying car with the truck during long-term movement under operating conditions.

Conclusion

Despite the lack of experience and statistics in the field of creation of quantomobiles in the world, the quantitative analysis of their energy consumption, in comparison with automobiles, has proved to be possible. The theory of Superunification, acting to overcome gravity and inertia forces, will undoubtedly be further developed and improved. However, as we speak, this theory can become the basis of design methods and engineering solutions for future quantum engines and non-fuel vehicles, including ground vehicles.

References

Autorambler (2014). *KamAZ for Dakar: how the best truck in the world works.* Available at: https://autorambler.ru/novosti/kamaz-dlya-dakara-kak-ustroen-luchshiy-gruzovik-v-mire-29-12-2014.htm. (accessed on: 18.10.2018) (in Russian)

Branderburg, J. (2017). *GEM Theory of QV-Thruster.* Available at: http://ssi.org/wp-content/uploads/2017/02/ssi_estes_park_proceedings_201609.pdf. (accessed on: 18.10.2018)

Davies, P. (1985). *Superforce*. New York: Touchstone.

Dirac P. (1927). The quantum theory of the emission and absorption of radiation. In: *Proceedings of the Royal Society of London. Series A, Containing Papers of a Mathematical and Physical Character*, 114. DOI: 10.1098/rspa.1927.0039

Dirac P.A.M. (1930). The Principles of Quantum Mechanics. Oxford: The Clarendon Press.

Einstein A. (1963). *Unified Field Theory. Collected scientific works.* Moscow: Nauka, vol. 2, pp. 286–301.

Fetta, G. (2014). *Electromagnetic Thruster. Patent US 2014 013724 A1.* Available at: http://www.rexresearch.com/fetta/US2014013724A1.pdf. (accessed on: 18.10.2018)

Heaviside, O. (1893). *Electromagnetic Theory, volume 1.* London: "The Electrician" Printing and Publishing Company, Limited, p.526.

Kotikov, Ju., Lozhkin, V.N. (2006). *Transportnaia energetika [Transport energetics].* Moscow: Publishing Center "Academia",

p.272. (in Russian)

Kotikov, Ju. (2018a). Structural properties and operational philosophy of the vehicle with the quantum engine. *Architecture and Engineering*, 3 (1), pp. 13–20. DOI: 10.23968/2500-0055-2018-3-1-13-20.

Kotikov, Ju. (2018b). Stages of Quantomobile Development. *Architecture and Engineering*, 3 (2), pp. 26–35. DOI: 10.23968/2500-0055-2018-3-2-26-35.

Leonov, V.S. (2002). Patent No. 2185526 (Russian Federation). S*posob sozdaniia tiagi v vakuume i polevoi dvigatel dlia kosmicheskogo korablia (varianty) [A method of thrust generation in vacuum and a field engine for spaceship (options)].* Bulletin No. 20 dd. 20.07.2002 (priority date: 21.05.2001). (in Russian)

Leonov, V.S. (2010a). *Quantum Energetics. Volume 1. Theory of Superunification*. Cambridge: Cambridge International Science Publishing, p.45.

Leonov, V.S. (2010b). *Kosmos: rezultaty ispytanii kvantovogo dvigatelia dlia sozdaniia tiagi bez vybrosa [Space: quantum engine test results regarding thrust generation without ejection].* Available at: http://www.astronomy.ru/forum/index.php/topic,77730.0.html. (accessed on: 28.01.2018) (in Russian)

Leonov, V.S. (2018). *Osnovy teorii reaktivnoj i nereaktivnoj tyagi [Fundamentals of the theory of reactive and non-reactive thrust].* Moscow: Armita. (in Russian)

McCulloch, M. (2014). *Physics from the Edge: A New Cosmological Model for Inertia.* Singapore: World Scientific Publishing Company.

Parker, B. (1991). *Mechta Einshteina. V poiskakh edinoi teorii stroeniia Vselennoi [Einstein's dream. The search for a unified theory of the Universe]* (translated from English by V. I. and O. I. Matsarskikh). Moscow: Nauka. (in Russian)

Petrov, A. (2015). *Rossiia uspeshno ispytala antigravitatcionnyi dvigatel Leonova [Russia successfully tested the Leonov anti-gravity engine].* Available at: http://www.km.ru/science-tech/2015/01/16/nauka-i-tekhnologii/753573-rossiya-uspeshno-ispytalaantigravitatsionnyi-dvi (accessed on: 28.09.2018) (in Russian)

Puthoff, H. (2010). Advanced Space Propulsion Based on Vacuum (Spacetime Metric) Engineering. *JBIS*, 63, pp. 82–89.

Tesla, N. (2009). *Patents. Samara.* Samara: Agni Publishing House.

Sanyuk, V.I., Sukhanov, A.D. (2009). *Dirac in 20th century physics: a centenary assessment.* Moscow: Russian University of Peoples Friendship.

Shawyer, R. (2006). *A Theory of Microwave Propulsion for Spacecraft. Satellite Propulsion Research Ltd 2006.* Available at: https://www.newscientist.com/data/images/ns/av/shawyertheory.pdf. (accessed on: 19.10.2018)

Tajmar M., Kößling M., Weikert M., Monette M. (2018). *The SpaceDrive Project – First Results on EMDrive and Mach-Effect Thrusters.* Available at: https://tu-dresden.de/ing/maschinenwesen/ilr/rfs/ressourcen/dateien/forschung/folder-2007-08-21-5231434330/ag_raumfahrtantriebe/SPC-The-SpaceDrive-Project-First-Results-on-EMDrive-and-Mach-Effect-Thrusters.pdf?lang=en. (accessed on: 19.10.2018)

Veinik A.I. (1991). *Termodinamika realnykh protcessov [Thermodynamics of real processes].* Minsk: Nauka i Tekhnika, 576 p. (in Russian)

ESTIMATION AND PREDICTION OF THE EFFECT OF ALTERNATIVE ENGINE TECHNOLOGIES AND POLICY MEASURES ON THE AIR QUALITY IN ST. PETERSBURG IN 2010–2030

Olga Lozhkina[1,2], Vladimir Lozhkin[2], Leonidas Ntziachristos[3]

[1] Saint Petersburg University of State Fire Service of EMERCOM of Russia
Moskovskiy Prospekt, 149, Saint Petersburg, Russia

[2] Solomenko Institute of Transport Problems of the Russian Academy of Sciences
12th Line of Vasilyevsky Island, 13, Saint Petersburg, Russia

[3] School of Mechanical Engineering of the Aristotle University of Thessaloniki
PO Box 458, Thessaloniki, GR 541 24, Greece

[1] olojkina@yandex.ru

Abstract

TProblems related to the quality of life in big cities are increasingly relevant, especially with regard to environmental issues. Motor transport is responsible for pollutant emissions and noise that decisively affect life in modern cities. In this context, evaluating, monitoring and forecasting urban environmental quality in short-term and long-term perspective has become an important issue for decision making and planning of sustainable cities. Computational model COPERT was applied in the study to obtain long-term projections of road transport-related emission rates for pollutants and greenhouse gases.

Three scenarios for St. Petersburg considering the population size, vehicle fleet structure, travel behavior, and fuel consumption are developed. It is shown that the greatest effect in emission reduction can be achieved through modernization of the vehicle fleet. Additional environmental protection measures such as an increase in the share of alternative fuels and promotion of public transportation are expected to result in an additional decline of pollutants and GHG emissions by 7–20% and 5–7%, respectively, in comparison with the Basic Scenario.

Keywords

Road transport, sustainable development, air pollution, short-term and long-term forecasting.

Introduction

Monitoring and improving air quality in built environment and cities are of crucial importance in the Russian Federation and all over the world (Franco et al., 2016; Genikhovich and Sciermeier, 1995; Genikhovich et al., 2002; Jain and Tiwari, 2016; Khreis et al., 2018; Lehtomäki et al., 2018; Lozhkin et al., 2013; Ni et al., 2018; Silva and Mendes, 2012; Singh et al., 2014; Taha, 2015; Zachariadis and Kouvaritakis, 2003; Yumino et al., 2015). Having ratified the Kyoto Protocol, the Convention on Long-Range Transboundary Air Pollution (CLRTAP) and other international acts, the Russian Federation confirmed its adherence to the concept of sustainable development and its intention to produce a considerable reduction in air pollutants and greenhouse gas (GHG) emissions.

Some progress has been achieved in reducing of vehicle-related air pollution through the application of strict Euro emission standards (Lozhkina and Lozhkin, 2015). However, we are still far from our objective to achieve such levels of air quality in big cities, like St. Petersburg, that do not exert a significant impact on the human health and the environment.

The results of our investigations (Lozhkina and Lozhkin, 2015, 2016) as well as the official data of the Committee for Nature Use, Environmental Protection and Ecological Safety of the Government of St. Petersburg (The

Committee on Environment Management, Environmental Protection and Ecological Safety of the Government of St. Petersburg, 1998, 2016) reveal that the city is periodically exposed to enhanced levels of nitrogen oxides (NOX), particulate matters (PM10 and PM2.5), carbon oxide (CO) and ozone (O3), and the road transport has been playing a key role in the air pollution of St. Petersburg since 1993, contributing to 75–85% of total pollutants and GHG emissions.

This is due to the continuous motorization that resulted in increasing the number of vehicles from 427,003 in 1993 to 1,063,500 in 2003 and 1,982,843 in 2013 (Report, 1998, 2016).

Real-time measurements and computational modeling represent complementary methods in air quality control and research. Air quality modeling enables not only real-time computational monitoring but also prediction and testing of future scenarios involving environmentally-friendly technologies and policy measures in the transport sector. The aim of the present study was to estimate and predict the effect of alternative technologies and policy measures in road transport-related emissions reduction on the air quality in St. Petersburg in 2010–2030 using the COPERT modeling system.

Methodology and input data collection

The COPERT methodology and software were used in this study to estimate the effect of alternative engine technologies and policy measures on the air quality in St. Petersburg in short-term and long-term perspective up to 2030.

COPERT is a European tool to calculate emissions from road transport (Ntziachristos et al., 2009; Zachariadis and Samaras, 1999). It is a part of the EMEP/CORINAIR Atmospheric Emissions Inventory Guidebook used by EU member states for official air emission inventorying. COPERT is also widely used around the world in air quality studies and academic research (Fontaras et al., 2014; Franco et al., 2016; Lozhkina and Lozhkin, 2015, Ni et al., 2018).

The COPERT methodology has the following advantages allowing achieving the aim of the present study: emission factors for more than 450 individual vehicle types including present and future hybrid and Euro 6 vehicles; estimates for a wide range of pollutants and GHG, including CO, NOX, volatile organic compounds (VOCs), particulate matter (PM), NH_3, CH_4 (calculated on the basis of vehicle emission factors), CO_2, SO_2 and heavy metals Pb, Cd, Cr, Cu, Ni, Zn, Se (estimated through the amount of fuel consumed). It also permits to analyze hot and cold emissions and emissions due to the evaporation of non-methane volatile organic compounds (NMVOCs).

Statistics on the vehicle fleet structure and vehicle age were gained from the Vehicle Market of Russia (2010, 2015, 2017). Average values of annual vehicle mileage were determined based on driver polling. Average seasonal meteorological parameters for St. Petersburg were taken from the official site of the Russian Meteorological Service (www.meteorf.ru).

Taking into account that the Russian vehicle fleet differs from the European one due to a large use of national vehicle brands, we modified emission factors for some pollutants (NO_X, CO, PM_{10}) according to the Russian data.

Various scenarios of road transport development in St. Petersburg in long-term perspective up to 2030
Current state of the road transport sector

The main gap in the activity data in the sector of motor transport is the lack of information on distribution of vehicles by emission technologies and absence of available statistics on fuel consumption.

Table 1 shows patterns in the vehicle fleet composition in St. Petersburg across a range of years.

Passenger cars have accounted for around four-fifths of all motor vehicles since 2004 and continue to be the main contributor to pollutants and GHG emissions.

The analysis of the data reveals that the passenger car fleet continued to grow more quickly than any other vehicle type, multiplying by a factor of 1.78 from 2003 to 2013. The peak was in 2013. In 2014–2015, the number of cars slightly fell, and then, in 2016, it began to increase again.

The fleet of HDV also saw the largest increase in 2013 and in 2017 (Table 1). The number of buses and coaches

Table 1. Vehicle fleet structure in St. Petersburg, 2004–2017.

	2004	2005	2006	2007	2008	2009	2010
Passenger cars	980,800	1,013,600	1,063,500	1,165,600	1,284,600	1,388,800	1,462,367
Trucks	104,841	106,170	114,663	121,731	122,458	117,231	129,043
Buses	18,735	19,550	21,792	23,757	22,400	22,030	22,714
Total	1,104,376	1,139,320	2,231,955	1,311,088	1,429,458	1,528,061	1,614,124
	2011	2012	2013	2014	2015	2016	2017
Passenger cars	1,525,967	1,537,437	1,741,867	1,670,794	1,638,183	1,676,379	1,710,811
Trucks	138,967	201,033	220,067	207,975	217,738	214,003	223,662
Buses	20,965	22,449	21,513	22,054	20,221	19,659	29,843
Total	1,685,899	1,760,919	1,983,447	1,900,823	1,876,142	1,910,041	1,964,316

Olga Lozhkina, Vladimir Lozhkin, Leonidas Ntziachristos — Pages 31–35

ESTIMATION AND PROJECTION OF THE EFFECT OF ALTERNATIVE ENGINE TECHNOLOGIES AND
POLICY MEASURES ON THE AIR QUALITY IN ST PETERSBURG OVER 2010-2030

DOI: 10.23968/2500-0055-2018-3-4-31-35

was more or less the same across 2004–2016 and sharply grew by 1.5 times in 2017.

Analysis of national plans for transport development

In the field of reducing motor transport-related air pollution, several legislative and technological measures were implemented nationwide. In 2003, the Federal Law on Banning Production and Use of Leaded Gasoline in the Russian Federation entered into force. In 2005, a direct step-by-step introduction of EU Vehicle Emission Standards was initiated, namely, the application of Directive 98/69/EC of the European Parliament and of the Council of 13 October 1998 was approved by the Russian Federation Government Decree No. 609 dated 12.10.2005 concerning Requirements to Harmful Emissions from Vehicles Produced in the Russian Federation.

Then, in 2008, technical regulations "Requirements to Automobile and Aviation Gasoline, Diesel and Ship Fuel, Jen Engine Fuel and Furnace Boiler Oil", harmonized with Directives 98/70/EC, 2005/55/EC and also aimed at the reduction of the transport's damaging effect on air quality, were introduced.

The implementation schedule of emission and fuel Standards in the Russian Federation is presented in Table 2.

Table 2. Implementation schedule of the emission and fuel standards in the Russian Federation.

Emission standards		Fuel standards	
Euro 2	2005	Euro 2	2005
Euro 3	2010	Euro 3	2013
Euro 4	2013	Euro 4	2015
Euro 5	2015	Euro 5	2016

In 2008, the Transport Strategy of the Russian Federation up to 2030 was approved by the Government of the Russian Federation. One of its priority goals is to reduce the harmful impact of transport on the environment by 2030 by increasing the use of alternative fuels and expanding the vehicle fleet with hybrid, electric and hydrogen vehicles.

Scenarios of motor transport development: assumptions and reasons behind their selection

This section provides an overview of some of the key factors that explain assumptions and reasons behind scenario development.

Over the last years, there has been a steady growth in population of St. Petersburg from 4,899,000 inhabitants in 2010 to 5,282,000 inhabitants in 2016. We suppose that it will continue to grow in the future.

Since motor transport is the main means for people and goods transportation in the city, we assume that the fleet will generally tend to increase by 2030, even though some fluctuations in road traffic levels may occur because of changes in the economy (including GDP) and disposable incomes of people, affecting car ownership and travel behavior of car owners. Table 3 presents actual and projected increase in the number of vehicles in St. Petersburg in 2010–2030.

The projections presume the assumptions around the current rates of economic and population growth, take-up of certain technologies and impacts of current government policies will remain valid.

The projections do not attempt to account for inevitable, but as yet unknown, changes that will occur in technology, energy demand and supply, and the international and domestic economy. The main assumption of all scenarios is progress in reducing pollutants and GHG emissions from motor vehicles in 2010–2030 through technological and fuel measures and through the growth of public transportation.

The main considerations are as follows: growth of the vehicle fleet (Table 3), modernization of the vehicle fleet over the projected period according to the implementation schedule of emission and fuel standards in the Russian Federation (Table 2).

The following three scenarios were developed by the authors:

1) Basic Scenario (Business-as Usual scenario): implementation of the main considerations listed above with the share of alternative fuels about 1.5–3%.

2) Scenario 2 (Bio scenario) considering all assumptions of the Basic Scenario and some additional

Table 3. Actual and projected increase in the number of vehicles in St. Petersburg in short-term and long-term perspective.

	2010	2015	2020	2025	2030
Passenger cars	1,470,490	1,850,000	1,950,000	2,100,000	2,250,000
Trucks	126,531	160,000	210,000	220,000	220,000
Buses	21,525	22,000	24,000	24,000	24,000
Total	1,618,546	2,032,000	2,454,000	2,619,000	2,834,000

Table 4. Main indicators of Scenario 2, developed considering the National Transport Strategy.

	2010	2011	2015	2018	2020	2024	2030
Share of alternative fuels, %	3	4	9	14	20	26	30
Share of vehicles with hybrid, electric and hydrogen engines	< 1	< 1	16	24	29	39	54

measures proposed in the Transport Strategy of the Russian Federation up to 2030 (Table 4).

3) Scenario 3 (Public Transportation + Fleet Modernization scenario): Basic Scenario plus an increase in the share of public transportation by 5% in 2015, 7% in 2020, 9% in 2025 and 12% in 2030 in respect to the Basic Scenario. The forecast starts from the base year of 2010 and projects emission rates of major pollutants and GHG for every 5 years up to 2030.

Results and discussion

The results of the numerical investigations show that we may expect a decline in the exhaust emissions from road transport by 2030. With the projected increase in the number of vehicles by a factor of 1.75 by 2030 compared to the base year of 2010, the greatest environmental effect could be achieved through faster introduction of stricter Euro 4–Euro 5 emission standards and stricter Euro 4–Euro 5 fuel quality standards (Basic Scenario).

The modeled trends show the reduction of greenhouse gas emissions (N_2O by a factor of 9 and CH_4 by a factor of 1.2–1.5) and the reduction of pollutant emissions (CO by a factor of 3, VOC and NMVOC by a factor of 2, NH_3 by a factor of 1.4, PM by a factor of 2. The NO_x emissions rate is expected to remain at the same level.

A continuous increase in the share of passenger cars and buses operating on compressed natural gas (CNG) and biodiesel by 30% by 2030, as indicated in the National Transport Strategy (Scenario 2), could lead to the reduction of greenhouse gas emissions, namely, CO_2 by 11% and N_2O by 12%. As to pollutants, their emissions are expected to be reduced by 7.6% in respect to CO, by 1.8% in respect to NO_x, by 20% in respect to VOCs, and they are also expected to grow for NH_3 and CH_4 by 3 and 4%, respectively, in comparison with 2030 in the Basic Scenario.

The use of diesel fuel corresponding to the Euro 5 quality standard would reduce SO_2 emissions by a factor of 2–2.5 in 2030 compared to the base year of 2010 (Scenarios 1–3).

Emissions of heavy metals Pb, Cd, Cu, Cr, Ni, Se Zn, as calculated by COPERT, would increase approximately by a factor of 1.5–2 between 2010 and 2030.

Conclusions

In recent twenty years, the number of motorized vehicles in St. Petersburg has risen sharply, but, thanks to some legislative and technological measures as well as to the increase of the purchasing capacity, there was considerable vehicle fleet modernization in the city over the last five years that resulted in the improvement of air quality.

The results of the numerical investigations also confirm this positive trend and show that a remarkable environmental effect could be achieved through faster modernization of the fleet with vehicles corresponding to Euro 4–Euro 6 emission standards and promotion of high-quality fuels.

Additional environmental protection measures such as an increase in the share of alternative fuels and promotion of public transportation are expected to result in an additional decline of pollutants and GHG emissions by 7–20% and 5–7%, respectively, in comparison with the Basic Scenario. It is evident that uncertainties are significant in long-term perspective. However, it is notable that, despite these uncertainties, our main conclusions are robust.

Acknowledgements

References

Analytical Agency ''Avtostat'' (2011). Vehicle Market of Russia in 2010, p.208. (in Russian)

Analytical Agency ''Avtostat'' (2016). Vehicle Market of Russia in 2015, p. 256 (in Russian)

Fontaras, G., Franco, V., Dilara, P. et al. (2014). Development and review of Euro 5 passenger car emission factors based on experimental results over various driving cycles. *Sci Total Environ*., 15, pp. 468–469. DOI: 10.1016/j.scitotenv.2013.09.043.

Franco, V., Zacharopoulou, T., Hammer, J. et al. (2016). Evaluation of Exhaust Emissions from Three Diesel-Hybrid Cars and Simulation of After-Treatment Systems for Ultralow Real-World NO_x Emissions. *Environ Sci Technol.,* 50 (23), pp. 13151–13159. DOI: 10.1021/acs.est.6b03585.

Genikhovich, E.L., Gracheva, I.G., Onikul, R.I., Filatova, E.N. (2002). Air pollution modeling at urban scale - Russian experience and problems. *Water, Air & Soil Pollution: Focus,* 2 (5-6), pp. 501–512. DOI: 10.1088/1742-6596/772/1/012031.

Genikhovich, E.L., Sciermeier, F.A. (1995). Comparison of United States and Russian complex terrain diffusion models developed for regulatory applications. *Atmos. Environ*., 29 (17), pp. 2375–2385. DOI: 10.1016/1352-2310(95)00053-2.

Jain, D., Tiwari, G. (2016). How would the present have looked like? Impact of non-motorized transport and public transport infrastructure on travel behavior, energy consumption and CO_2 emissions. *Sust. Cities and Society,* 22, pp. 1–10. DOI: 10.1016/j.scs.2016.01.001.

Khreis, H., de Hoogh, K., Nieuwenhuijsen, M.J. (2018). Full-chain health impact assessment of traffic-related air pollution and childhood asthma. *Environ Int*., 114, pp. 365–375. DOI: 10.1016/j.envint.2018.03.008.

Klein, T., Kukkonen, J., Baklanov, A. et al. (2012). Interactions of physical, chemical, and biological weather calling for an integrated approach to assessment, forecasting, and communication of air quality. *Ambio,* 41 (8), pp. 851–864. DOI: 10.1007/s13280-012-0288-z.

Lehtomäki, H., Korhonen, A., et al. (2018). Health Impacts of Ambient Air Pollution in Finland. *Int J Environ Res Public Health*., 15 (4). DOI: 10.3390/ijerph15040736.

Lozhkin, V.N., Lozhkina, O.V., Ushakov, A. (2013). Using K-Theory in Geographic Information Investigations of Critical-Level Pollution of Atmosphere in the Vicinity of Motor Roads. *World Applied Sciences Journal*, 23 (13), pp. 96–100.

Lozhkina, O.V., Lozhkin V.N. (2015). Estimation of road Transport related air Pollution in Saint Petersburg using European and Russian calculation Models. T*ransport. Res. Part D*, 36, pp. 178–189. DOI: 10.1016/j.trd.2015.02.013.

Lozhkina, O.V., Lozhkin, V.N. (2016). Estimation of nitrogen oxides emissions from petrol and diesel passenger cars by means of on-board monitoring: Effect of vehicle speed, vehicle technology, engine type on emission rates. *Transport. Res. Part D*, 47, pp. 251–264. DOI: 10.1016/j.trd.2016.06.008.

Ni, Z.Z., Luo, K. et al. (2018). Assessment of winter air pollution episodes using long-range transport modeling in Hangzhou, China, during World Internet Conference, 2015. *Environ Pollut.,* 236, pp. 550–561. DOI: 10.1016/j.envpol.2018.01.069.

Ntziachristos, L., Gkatzoflias, D., Kouridis, Ch., Samaras Z. (2009). COPERT: A European Road Transport Emission Inventory Model. In: *Proceedings of the 4th International ICSC Symposium on Information Technologies in Environmental Engineering*, pp. 491–504. DOI: 10.1007/978-3-540-88351-7_37.

Silva, L.T., Mendes, J.F.G. (2012). City Noise-Air: An environmental quality index for cities (Review). *Sust. Cities and Society,* 4 (1), pp. 1–11. DOI: 10.1016/j.scs.2012.03.001.

Singh, V., Sokhi, R.S., Kukkonen, J. (2014). PM2.5 concentrations in London for 2008 - a modeling analysis of contributions from road traffic. *J Air Waste Manag Assoc*., 64 (5), pp. 509-518. DOI: 10.1080/10962247.2013.848244.

The Committee on Environment Management, Environmental Protection and Ecological Safety of the Government of St. Petersburg (1998). *Report on Environmental situation in St. Petersburg and Leningrad Region in 1997*. (Leningrad: Lencomecologhia) (in Russian)

The Committee on Environment Management, Environmental Protection and Ecological Safety of the Government of St. Petersburg (2016). *Report on Environmental situation in St. Petersburg in 2015*. Available at: http://www.infoeco.ru/assets/files/Doklad/doklad_2015.pdf (accessed on 15.02.2018) (in Russian)

Taha, H. (2015). Meteorological, air-quality, and emission-equivalence impacts of urban heat island control in California. *Sust. Cities and Society,* 19, pp. 207–221. DOI: 10.1016/j.scs.2015.03.009.

Yumino, S., Uchida, T., et al. (2015). Total assessment for various environmentally conscious techniques from three perspectives: Mitigation of global warming, mitigation of UHIs, and adaptation to urban warming. *Sust. Cities and Society,* 19, pp. 236–249. DOI: 10.1016/j.scs.2015.05.010.

Zachariadis, T., Kouvaritakis, N. (2003). Long-term outlook of energy use and CO2 emissions from transport in Central and Eastern Europe. *Energy Policy,* 31 (8), pp. 759–773. DOI: 10.1016/S0301-4215(02)00126-X.

Zachariadis, T., Samaras, Z. (1999). An Integrated Modeling System for the Estimation of Motor Vehicle Emissions. *J Air Waste Manag Assoc*., 49 (9), pp. 1010–1026. DOI: 10.1080/10473289.1999.10463892.

SURFACE ACTIVATION OF THE REINFORCING FILLER AND POLYMER MATRIX MODIFICATION AS EFFICIENT WAYS TO UPGRADE PROPERTIES OF POLYMER-MATRIX COMPOSITES BASED ON EPOXY MATRICES

Anton Mostovoy[1], Sergey Arzamastcev[2], Yulia Kadykova[2], Igor Danilov[3], Arthur Asoyan[4], Alexey Marusin[5]

[1] Engels Technological Institute (branch of SSTU)
Freedom square, 17, Engels, Russia

[2] Yuri Gagarin State Technical University of Saratov (SGTU)
Politechnicheskaya street, 77, Saratov, Russia

[3] Peoples' Friendship University of Russia
Miklukho-Maklaya Street, 6, Moscow, Russia

[4] Moscow Automobile and Road Construction State Technical University (MADI)
Leningradsky Prospect, 64, Moscow, Russia

[5] Saint Petersburg State University of Architecture and Civil Engineering
Vtoraja Krasnoarmejskaja ul., 4, St. Petersburg, 190005, Russia

[5] 89312555919@mail.ru

Abstract

The article is devoted to issues of interaction rise in the system "polymer matrix — reinforcing filler," which provides an increase in the complex of composite properties. Both surface activation of the reinforcing filler and polymer matrix modification are considered as options. It has been demonstrated that the number of functional groups available for interaction at the surface of basalt fibers increases due to desizing and surface activation of the fibers, which provides an increase in the complex of basalt fiber reinforced polymer properties.

It has been found that the use of different methods of surface activation allows providing high strength characteristics of carbon-, glass-, and basalt fiber reinforced polymers, exceeding similar characteristics of materials in which surface activation of the reinforcing filler was not performed. Experiments have proved that the use of unidirectional carbon fibers for reinforcement leads to a significant increase in the entire complex of mechanical properties, due to the possibility to realize stress-strain properties of the reinforcing filler to the limit.

Keywords

Reinforcement, basalt fiber reinforced polymer, carbon fiber reinforced plastic, surface activation.

Introduction

In recent decades, a substantial growth of the production of composite materials reinforced with chemical fibers has been observed. This is due to their high performance, low weight, and high corrosion resistance. The entirety of characteristics determines a vast scope of applications for such materials, starting from household application and ending with their use in the defense industry, aircraft and rocket production, and space industry, where a persistent struggle for weight reduction of structures exists (Barile et al., 2019).

Epoxy resins are the most common and universal of the whole family of resins, representing one of the best types of binding agents used in the production of fiber-reinforced composite materials, due to a number of valuable properties: high dielectric index, mechanical strength, water resistance, low shrinkage during the transition to the cross-linked state, good adhesion to metals, porcelain, glass (Singla, Chawla, 2010).

The range of chemical fibers used for reinforcement has significantly narrowed for a number of reasons. Glass, basalt and carbon fibers are in most common use today
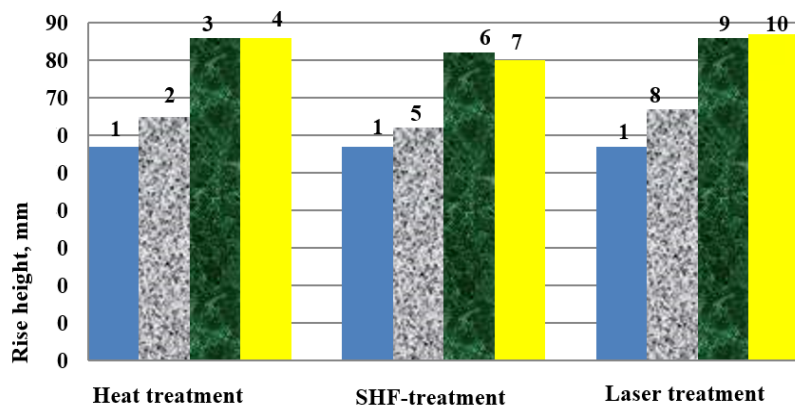
Figure 1. Change in wettability of basalt fibers with a mixture of monomers depending on the type of modification:
1 – untreated fiber; 2, 3, 4 – heat-treated fiber at 200, 250, 300ºC, respectively; 5, 6, 7 – SHF-treated fiber within 2, 3, 4 minutes, respectively; 8, 9, 10 – laser-treated fiber within 1, 2, 3 seconds, respectively

(EL-Wazery, 2018; Matveeva, Lebedev, 2018; Gerasimova et al., 2018).

The important task of high-strength reinforced epoxy composites manufacture is to create conditions for chemical or physical-and-chemical interaction in the system "reinforcing filler — polymer matrix" (Colson et al., 2018).

This interaction is usually prevented by sizing and finishing agents applied to the fiber surface during its production. One way to increase the interaction force between the polymer matrix and the fiber is surface activation of the reinforcing fiber (Baloji Naik et al., 2014; Tijana et al., 2014; Molina, 2016).

Subject, objectives, and methods

The subject of the research was to increase interaction in the system "polymer matrix — reinforcing fiber." The objective of the research was to determine methods of surface activation of reinforcing fibers and polymer matrix modification in order to upgrade the complex of reinforced composites properties.

The epoxy resin ED-20, such hardening agents as polyethylene polyamine (PEPA) and PO-300, such plasticizing agents as trichloroethyl phosphate (TCEP) and tricresyl phosphate (TCP) were used as objects of the research.

The choice of TCEP and TCP is based on the presence of flame retarders in their composition — phosphorus and chlorine, which structure the epoxy polymer at elevated temperatures and increase the yield of carbonized structures, which, in turn, form a physical barrier to the interdiffusion of combustible gases and an oxidant in the combustion zone, reducing the flammability of the epoxy composite (Wenchao et al., 2014).

Basalt fibers produced by the Grafit R&D establishment (Moscow), OAO Ivotsteklo (Ivot, Bryansk Region), OOO Kombinat Volna (Krasnoyarsk), and ZAO Belichsky Zavod Teplozvukoizolyatsiya (Irpin, Ukraine), as well as the UT-900Р (УТ-900П) carbon fabrics were used as reinforcing materials. Analyses of composite properties were carried out by standard methods.

Results and discussion

The efficiency of the oxidative method for increasing the activity of the carbon fiber surface was experimentally proved since the mechanical, physical-and-chemical, and chemical properties exceeded the similar characteristics of carbon fiber reinforced polymer samples based on the non-activated fiber (Table 1).

Table 1. Properties of the carbon fiber reinforced polymer based on the epoxy matrix reinforced with the untreated and activated carbon fiber.

Carbon fiber type	Density, kg/m^3	Oxygen index, %	Water absorption in case of boiling within 2 hours, %	Break point in shear, MPa	Break point under bending, MPa	Brinell hardness, MPa
Untreated	1,350	62	0.55	14	600	596
Activated	1,428	66	0.41	14	645	627

Basalt fibers modification by these methods affects the parameters of their porous structure. An increase in the maximum adsorbed volume and pore diameter for all types of basalt fiber modification, in comparison with untreated basalt fibers, is observed for fibers produced by the Grafit R&D establishment (Moscow) and OAO Ivotsteklo (Ivot, Bryansk Region). At the same time, the used methods of modification do not cause significant changes in the structure of fibers produced by OOO Kombinat Volna (Krasnoyarsk) and ZAO Belichsky Zavod Teplozvukoizolyatsiya (Irpin, Ukraine).

These results are associated with differences of sizing agents applied to fibers. For example, the fibers of the Ukrainian and Krasnoyarsk manufacture were treated with the "active" sizing agent creating an oleophilic film on the surface, and the fibers produced by the Grafit

R&D establishment and OAO Ivotsteklo were treated with the "inert" sizing agent which gives the fiber surface oleophobic properties.

The presence of the oleophobic sizing agent on the surface of the BF causes a decrease in the physical-and-chemical interaction between basalt fibers and monomers, which leads to an increase in water absorption and a decrease in physical and mechanical properties of basalt fiber reinforced polymers (Table 2).

The analysis of the obtained data shows that the physical-and-chemical as well as mechanical properties of basalt fiber reinforced polymers based on prepregs obtained by the method of polycondensation combination of components reinforced with modified basalt fibers produced by OAO Ivotsteklo exceed the similar indicators of basalt fiber reinforced polymers based on untreated fibers.

For example, for these basalt polymers reinforced with heat-treated and SHF-treated fibers, break point in shear, characterizing the adhesive interaction, increases. Brinell hardness increases by 15–20% with heat treatment and by 15% with SHF-treatment. Other indicators of basalt polymers reinforced with heat-treated fibers produced by the Grafit R&D establishment (Brinell hardness, impact value, and break point under bending and in shear) increase as well.

The increase in physical-and-chemical as well as mechanical properties of the obtained basalt fiber reinforced polymers on the basis of modified fibers indicates a more active interaction between the functional groups of modified basalt fibers, produced by OAO Ivotsteklo and Grafit R&D establishment, and phenol-formaldehyde oligomer. This state is achieved by desizing and surface activation of fibers with the presented modification methods, thanks to which the number of functional groups available for interaction at the surface of basalt fibers increases (Table 2).

The use of different methods of surface activation allows providing high strength characteristics of carbon-, glass-, and basalt fiber reinforced polymers, exceeding similar characteristics of materials employed usually (Table 3).

Modification of the polymer matrix is equally important for the upgrade of the complex of properties. Previously

Table 2. Physical-and-chemical as well as mechanical properties of basalt fiber reinforced polymers based on basalt fibers of different manufacturers.

Manufacturer	Modification	Brinell hardness, MPa	Break point under bending, MPa	Break point in shear, MPa	Impact value, kJ/m^2	Water absorption in case of boiling within 2 hours, %
Kombinat Volna Ltd.	-	503	600	14	329	0.26
	heat treatment	500	605	14	330	0.26
	SHF-treatment	500	600	14	320	0.25
Ivotsteklo OJSC	-	510	640	20	342	0.24
	heat treatment	614	683	27	385	0.23
	SHF-treatment	586	654	26	360	0.23
Belichsky Zavod Teplozvukoizolyatsiya CJSC	-	475	450	29	313	0.24
	heat treatment	470	453	18	315	0.25
	SHF-treatment	470	448	18	313	0.25
Grafit R&D establishment	-	233	422	12	190	0.33
	heat treatment	338	518	16	210	0.28

Table 3. Comparative characteristics of conventional structural and developed materials.

Indicator	Steel	Aluminum alloy	Glass basalt fiber reinforced polymer
Density, kg/m^3	7.8	2.7	1,8–1,9
Elasticity modulus, hPa	210	70	70
Strength limit, MPa	390	250	1,700
Temperature coefficient of linear thermal expansion, x 10^{-6}/°C	11.9–14.2	2.4	0.45–8.3
Corrosion resistance: - low - high - very high	X	X	X

developed epoxy compositions were used as a polymer matrix in preparation of composites based on carbon fabrics.

UT-900P carbon fabrics (carbonized) in the amount from 20 to 50 pts. wt. were introduced in the epoxy composition containing (for 100 pts. wt. of ED-20) 30 pts. wt. of plasticizing agents (trichlorethyl phosphate (TCEP) and tricresyl phosphate (TCP)) and 40 pts. wt. of PO-300 hardening agent. Carbon fiber molding was carried out

in two ways: fabrics proofing with the epoxy composition followed by hardening within 24 hours at the room temperature and heat treatment at 90ºC and 150ºC within 60 minutes (model samples) and compression molding at 150ºC and the pressure of 25 MPa.

The epoxy resin hardened with PO-300 is characterized by sufficiently high complex of properties (Table 4), in comparison with the epoxy resin hardened with PEPA; it is due to changes in density, the nature of spatial grid nodes

Table 4. Properties of epoxy composite model samples, plasticized with TCP.

Formulation of the composition hardened with 40 pts. wt. of PO-300, pts. wt.	Break point under bending, MPa	Impact value, kJ/m^2	Brinell hardness, MPa	Hardening degree, %	Oxygen index, % vol.
100 ED-20	76	13	185	98	19
100 ED-20 +50 UT-900P	162	51	292	85	-
70 ED-20 + 30 TCP	8*	36	-	84	-
100 ED-20+30 TCP + 20 UT-900P	147	33	83	86	42
100 ED-20+30 TCP + 30 UT-900P	140	51	98	86	42
100 ED-20+30 TCP + 40 UT-900P	138	60	130	86	45
100 ED-20+30 TCP+50 UT	174	50	83	86	45

* The coefficient of variation of properties — 5–10%.

Table 5. Properties of epoxy composites plasticized with TCEP.

Sample No.	Formulation of the composition hardened with 40 pts. wt. of PO-300	Break point under bending, MPa	Impact value, kJ/m^2	Brinell hardness, MPa	Hardening degree, %	Oxygen index, % vol.
1	100 ED-20 + 30 TCEP	4*	34	Not determined	84	30
2	100 ED-20 + 50 UT	162	51	292	85	-
3	100 ED-20+30 TCEP + 50 UT-900P	34*	162	110	86	60
4	100 ED-20+30 TCEP + 50 UT-900P	127*	91	-	90	50
5	100 ED-20+30 TCEP + 50 UT-900P	85*	76	130	88	50
6	100 ED-20+30 TCEP + 50 UT	182*	162	83	88	60

Note:
1. * samples do not destroy; deflection is equal to 1.5 of the sample thickness;
2. 3, 5, 6, 7 — model samples;
4 — a molded sample;
3. the coefficient of variation of properties — 5–10%.

as a result of changes in the chemical composition of the epoxy polymer through the use of a hardening agent containing polyamide links chemically related to the grid structure.

The introduction of TCP plasticizing agent increases the resistance to impact, and samples do not destroy during bending tests (Table 4). In estimating the influence of the reinforcing filler on composite properties, it was found that the introduction of carbon fabrics in the unplasticized epoxy resin doubles the resistance to bending and increases the resistance to impact by four times (Table 4).

Upon an increase in the content of carbon fabrics in the plasticized composition from 20 to 50 pts. wt., stress-strain properties to the degree of filling of 40 pts. wt. do not change significantly (Table 4).

The replacement of TCP plasticizer by TCEP (Table 5), also introduced in the amount of 30 pts. wt., provides a substantial increase in physical and mechanical properties: the impact value increases from 50 to 162 kJ/m^2, the samples do not destroy during bending tests at the bending stress value of 34 MPa.

Samples obtained by means of compression molding at the temperature of 150ºC are characterized by higher hardening degree of 90% (Table 3), which leads to a decrease in the impact value from 162 to 91 MPa, while the bending stress increases from 34 to 127 MPa.

The use of unidirectional carbon fibers for reinforcement (sample 6, Table 5) leads to a significant increase in the entire complex of mechanical properties, due to the possibility to realize stress-strain properties of the reinforcing filler to the limit. The developed carbon fiber reinforced polymers belong to the class of hard-burning materials and exceed the industrial carbon fiber reinforced polymers with similar fillers in terms of the level of their properties.

Conclusion

The experiments proved that regardless of the basalt fiber manufacturer, desizing and surface activation lead to an increase in physical-and-chemical as well as mechanical properties of the obtained basalt fiber reinforced polymers, which indicates a more active interaction between the functional groups of modified basalt fibers and epoxy oligomer. It was proved that the replacement of tricresyl phosphate by trichlorethyl phosphate in the composition of the obtained carbon fiber reinforced polymer allows increasing the strength characteristics of the material, and the oxygen index significantly.

References

Baloji Naik, R., Jagtap, S.B., Naik R.S., Malvankar, N.G., Ratna, D. (2014). Effect of non-ionic surfactants on thermomechanical properties ofepoxy. *Multiwall carbon nanotubes composites, Progress in Organic Coatings*, 77, pp. 1883–1889. DOI: 10.1016/j.porgcoat.2014.06.024.

Barile, C., Casavola, C., De Cillis, F. (2019). Mechanical comparison of new composite materials for aerospace applications. *Composites Part B: Engineering*, 162, pp. 122–128. DOI: 10.1016/j.compositesb.2018.10.101.

Colson, J. et al. (2018). Adhesion properties of regenerated lignocellulosic fibres towards poly(lactic acid) microspheres assessed by colloidal probe technique. *Journal of Colloid and Interface Science*, 532, pp. 819–829. DOI: 10.1016/j.jcis.2018.08.032.

EL-Wazery, M.S. (2018). Mechanical characterization of glass-basalt-carbon/polyester hybrid composites. *International Journal of Engineering, Transactions A: Basics*, 31 (7), pp. 1139–1145.

Gerasimova, V.M., Zubova, N.G., Ustinova, T.P. (2018). Effectiveness of Organosilane Modification of Basalt. *Fibre Chemistry*, 49 (6), pp. 357–359.

Matveeva, I.G., Lebedev, M.P. (2018). Polymer Composite Materials Based on Basalt. *Theoretical Foundations of Chemical Engineering*, 52 (4), pp. 670–672.

Molina, S. (2016). Modification of Natural Fibers Using Physical Technologies and Their Applications for Composites. *Lignocellulosic Fibers and Wood Handbook: Renewable Materials for Today's Environment*, pp. 323–344.

Singla, M., Chawla, V. (2010). Mechanical Properties of Epoxy Resin – Fly Ash Composite. J*ournal of Minerals & Materials Characterization & Engineering*, 9 (3), pp. 199–210.

Tijana, S. et al. (2014). Improvement of epoxy resin properties by incorporation of TiO_2 nanoparticles surface modified with gallic acid esters. *Materials and Design*, 62, pp. 158–167. DOI: 10.1016/j.matdes.2014.05.015.

Wenchao, Z. et al. (2014). The influence of the phosphorus-based flame retardant on the flame retardancy of the epoxy resins. *Polymer Degradation and Stability*, 109, pp. 209–217. DOI: 10.1016/j.polymdegradstab.2014.07.023.

ACCIDENT ANALYSIS OF LOW PRESSURE GAS DISTRIBUTION SYSTEMS

Alexander Shkarovskiy[1,2], Maciej Kotuła[3]

[1] Saint Petersburg State University of Architecture and Civil Engineering
Vtoraja Krasnoarmejskaja ul., 4, St. Petersburg, 190005, Russia

[2] Koszalin University of Technology
2 Sniadeckich St., 75-453 Koszalin, Poland

[3] Gas Supply Company in Kołobrzeg, Polish Gas Company Ltd.
30 Koszalińska St., 78-100 Kołobrzeg, Poland

[1] szkarowski@mail.ru

Abstract
In terms of safety, gas supply represents a highly important area of science and engineering. On the one hand, gas is a very convenient primary energy source for consumers. On the other hand, gas can be extremely dangerous for life and health of people, if strict requirements to design, construction and operation of gas supply systems are not complied with. The article reviews an accident that occurred in a small Polish city in 2010. We analyzed data from the Prosecutor's Office and relevant publications and questioned workers of the gas supply company. The article describes how an unlucky train of events resulted in a tragedy. The main circumstances were an unacceptable change in the gas distribution plant equipment and violation of operating rules, which resulted in an unauthorized pressure increase in a district network and internal systems designed for low pressure. We analyzed follow-up technical and administrative measures taken regarding the Polish gas supply system and compared some peculiarities of Polish and Russian gas technologies. The main purpose of the analysis is to prevent such accidents in future.

Keywords
Gas supply, safety, gas distribution plant, equipment, operation, pressure increase.

Introduction

The concept and main components of gas supply systems are similar in most countries. Therefore, accidents are also similar in their reasons, progress and consequences. The article presents results of an analysis of one such accident. Experts in design, construction and operation of gas supply systems can assess, on their own, how a combination of circumstances (however improbable) can result in a tragedy. This will probably allow avoiding such events through simple design, technological and administrative measures (Ansari et al., 2017).

Subject, objectives and methods

The accident analyzed in the article occurred on November 30, 2010 in small Polish city Zielona Góra with population about 140 thousand people, situated in the Lubusz province in Western Poland, close to the border with Germany. We can judge about the beginning of the accident based only on subjective and highly emotional statements of those affected who claimed that "...gas stoves in apartments started exploding one by one" (Super Express, 2010). If we assess those statements objectively, it was enough to try to light a gas-range burner

for a breakout of heavy fire that would be impossible to put out. Such fire was particularly the case when oven burners were attempted to be lit, where a burst of flame actually differed little from an explosion (Fu et al., 2018).

Let us think about the reasons why the fire could not be put out and what followed. Generally, we turn a stove knob, already holding a lit match or a stove lighter in the other hand, or (in modern models) simultaneously activating a spark igniter. In case of a strong burst of flame, a person jumps back, intuitively protecting himself from the flame. Obviously, the gas knob is left open. In modern ovens, a flame sensor can activate, but the outcome is the same. Panic prevents people from reaching the stove to close the gas knob or shut off the gas tap, the latter quite often being even less easy to reach (Kim et al., 2018).

The events swept three neighborhoods — Pomorskie (Pomeranian), Śląskie (Silesian) and Raculka, where the explosions resulted in three fires. Two of them were extinguished rather quickly, but the third one, which swept an apartment on the 8th floor in the Pomorskie (Pomeranian) neighborhood, followed a tragic scenario. Firemen fought against it for several hours and saved a woman cut off by the fire. However, a fifty-year-old man died in the fire. He probably had lost consciousness at the time of the explosion. 6,500 people were evacuated from the houses affected by the accident. One can easily imagine their mental state amidst the fires and the howl of fire-engines (Tymchik et al., 2018).

According to the Minister of the Interior and Administration, no such large-scale accident had ever happened in Poland. In terms of the number of victims, there had been even more tragic isolated accidents affecting an apartment, a stairwell or a residential building. Still, if we estimate the area affected by the accident, the number of houses and evacuated people, one cannot but agree with such estimation. The containment of the accident involved: 500 policemen (53 vehicles), 177 professional and volunteer firemen (47 vehicles), 35 city guards (two vehicles), 17 ambulance health workers, 100 emergency gas service specialists (50 vehicles), three emergency power supply service workers (1 vehicle), 10 specialists from the crisis management center, along with 17 city buses (Vasista, Alsudairi, 2018).

Results and discussion
1. Preliminary analysis

The reason of the accident remained unknown for a long time, as the investigation went on. However, it was not very difficult for specialists to make a preliminary conclusion that medium-pressure gas started to flow to the low-pressure gas distribution system. It started from a gas distribution plant (GDP) and went to the street network, and then to internal building systems.

When the gas supply system under consideration (1970–1980s) was constructed, gasification of populated areas developed in Poland similarly to that in the majority of other countries. Medium-pressure gas was supplied to stand-alone GDPs, and the built-up area was covered by a network of low-pressure gas pipelines. Such layout was considered to be safer. Considering that the maximum pressure upstream of household gas appliances should not exceed 2.5 kPa, the entire network was usually designed in the operating pressure range of 2.0...2.5 kPa.

Pipelines and equipment of such systems were under pressure of several bars, which was hundreds of times higher. Many system elements, such as taps, seals, supply hoses, might just fail to operate, which would result in gas contamination of premises, gas accumulation in ovens, etc. Suffice it to say that gas stoves have a certificate of gas density at pressure up to 3.0 kPa, and gas meters — up to 5.0 kPa. What happened when a person tried to light a burner was briefly analyzed above.

The very fact of medium-pressure gas entering the low-pressure gas system was clear to the specialists. Still, without necessary technical documentation, it was difficult even for scientists and skilled professionals in design and operation of gas supply systems to determine clear reasons.

The GDP design in any country would not allow medium pressure-gas to enter the exhaust gas pipeline. At least three devices prevent such entry: a pressure regulator itself and two safety valves — a safety shut-off valve and a safety discharge valve. Operating together, they should prevent outlet pressure from exceeding the established level (which in Russia, as a rule, is 20% higher than the maximum allowable level). The shut-off valve actuates when this happens. The discharge valve is adjusted for two times less value. This prevents an unjustified interruption of gas supply, which would be unavoidable at the shut-off device actuation.

There are few reasons for safety devices to actuate. Sometimes, at dramatic changes of the inlet pressure, dynamic performance of the pressure regulator may prove insufficient. Still, contamination of the pressure regulator valve seat is a more frequent reason — it should close completely if no gas is used, but this does not happen. The pressure regulator membrane can be damaged as well. The maximum pressure in low-pressure systems at the time of construction was 5 kPa. That is why, in any case, the shut-off valve should have actuated at a pressure not exceeding 6 kPa. Then what happened?

2. Prosecutor's Office data

Only at the end of the investigation when access to the documents was provided, specialists were able to begin a scientific analysis of accident causes. The authors of the article present their version of such analysis. In some cases, we are forced to deal with strict legal wordings and long sentences typical for Polish language, thus literal translation is complicated.

The first one of those wordings is the very title of the message dated January 18, 2013, posted on the official website of the Regional Prosecutor's Office: "The indictment against the gas distribution network master in the case of gas explosion in Zielona Góra neighborhood" (Prokuratura Okrégowa, 2013). Thus, the prosecutor's investigation translates the search for causes into the field of the human factor. Literal translation of the message is

impossible in principle, nor required for the goals of the analysis. However, we should stick to the common logic of the message.

The prosecutor submitted the indictment against the gas distribution network master to court. The indictment states that, being responsible for modernization of the gas distribution plant, he tolerated an incorrect connection of GDP elements and used improper materials. His actions resulted in the GDP failure to operate, which manifested in the fact that exceedingly high-pressure gas entered the gas distribution system, leading to de-pressurization of the GDP and network that supplied gas to individual consumers. Consequently, the actions of the person accused led to the natural gas explosion in one of the buildings, thus largely threatening lives and health of many citizens, and their property.

The investigation found that on 30.11.2010 an accident involving the pressure regulator occurred. Unacceptably high gas pressure resulted in de-pressurization of internal systems in the apartments and uncontrolled gas leaks. As a result, there were heavy bursts of flame and so-called (in the original language) explosions of stoves at attempts to use those, along with the accumulation of large amounts of gas in the premises.

In order to determine causes of the accident at the GDP, developing under this scenario, the investigation turned to experts. They provided several causes in their expert opinion:
- reduced diameter of the discharge pipeline;
- improper pipeline laying (siphon pipeline laying);
- no protection against precipitation;
- failure of the standby line shut-off valve (the valve trigger did not affect the shut-off mechanism).

Those three pieces of the Prosecutor's Office message provide a great deal of essential information to be analyzed. It goes without saying that the core reason for the tragedy was the failure of the pressure regulator. However, such equipment failures do happen in the gas

supply industry, like in any other engineering field. No tragic events happen at such failures, as gas distribution plants have a range of safety systems briefly described above (Wang, Yang, 2018).

Note the reference to the failure of the shut-off valve particularly in the standby line. This indicates that the main pressure reduction line was simply turned off. Brief information on the layout of the gas distribution plant designed more than 40 years ago is needed at this point. The GDP was constructed based on a two-line pressure reduction layout (Figure 1). Both pressure reduction lines are placed in the GDP building; they are fully functional and identical but for the equipment settings. They share only inlet and outlet shut-off and discharge units located outside the building, and the safety discharge valve.

3. Human factor

The authors had the opportunity to talk to the employees of this gas supply company. It turned out that at first the failure of the shut-off valve to actuate was named as the reason of the accident (although as rumor only). The materials of the prosecutor's investigation confirmed this assumption. However, based on the information received from the experts, the accident could be caused by an array of reasons that occurred simultaneously against the laws of probability.

The faults in GDP operation occurred during routine modernization of the equipment, that was performed through the efforts of the gas supply company. During the works, it was established that the safety shut-off valve on the main pressure reduction line did not operate properly. It was removed and placed under adjustment. The GDP was switched to the standby line for a long time.

It was this line where malfunction of the pressure regulator occurred. Most likely, it was due to a damaged membrane. This ultimately led to a spike in pressure downstream of the pressure regulator. An emergency situation occurred (which was still standard one), and
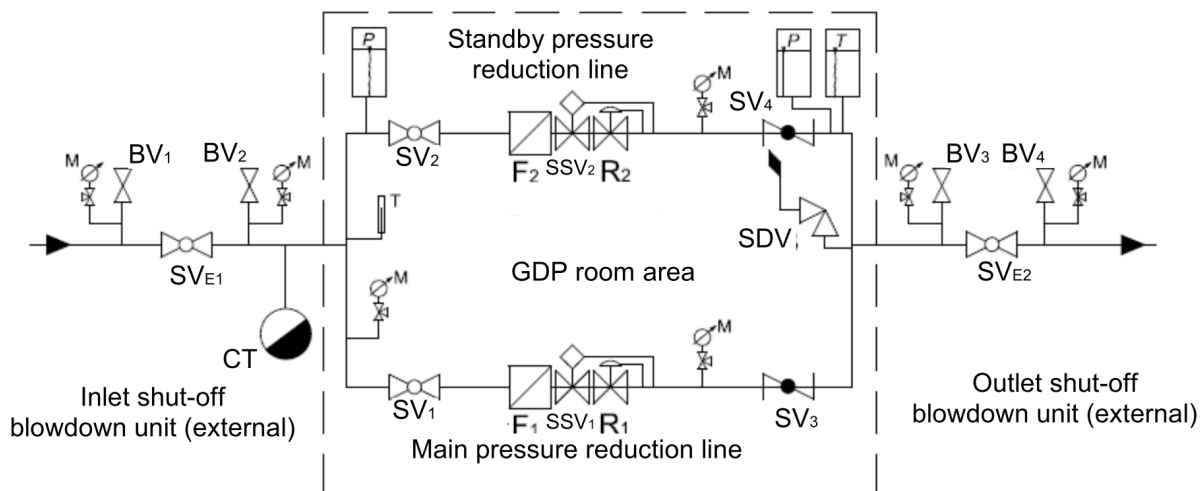

Figure 1. Layout of the low-pressure GDP with two pressure reduction lines:
SV — external shut-off valve; BV — blowdown valve; SV — shut-off valve; F — filter; SSV — safety shut-off valve;
R — pressure regulator; SDV – safety discharge valve;
M — manometer; T — temperature recorder; P — pressure recorder;
CT — condensate trap.

safety systems should have actuated in sequence. Further, we will consider how it should have happened if the GDP had been in a normal operating condition.

The GDP outlet design pressure and the operating pressure of the street network was 2.0 kPa. At the pressure of 2.7 kPa (standard settings of the equipment are provided herein), the spring safety discharge valve that is common for both lines should have actuated. In this case, gas would have been dumped into the atmosphere in the amount of up to 25% of the GDP capacity. In case of further increase in the outlet pressure to 2.9 kPa, the main line safety shut-off valve (SSV1) should have actuated, and the GDP would have automatically switched to the standby line. In case of further pressure increase, the standby line safety shut-off valve (SSV2) should have actuated at the pressure of 3.9 kPa, and gas would not have been supplied to the network anymore. The dumping of gas into the atmosphere through the safety discharge valve would have continued.

As can be seen, the situation would have ended in case of switching to the standby line, since the properly functioning pressure regulator would have started operating. But, as stated above, the GDP in question was not fully operational: *by that time, it operated through the standby pressure reduction line*, and both safety devices did not go off.

Speaking of the reasons behind the failure of the standby line safety shut-off valve to operate, it follows from the prosecutor's materials that its "trigger did not affect the shut-off mechanism". The authors managed to establish that the valve was just irresponsibly disabled.

According to the employees of the gas supply company, after the GDP switched to the standby line, it was often off — the safety shut-off valve actuated, and gas supply to consumers stopped. To avoid unwarranted interruptions in gas supply, the trigger of the safety shut-off valve was simply disabled physically, in the hope of sufficient safety ensured by the safety discharge valve.

4. Issues with the safety discharge valve

The findings of the prosecutor's investigation touch upon not the safety shut-off valve but its piping. By the end of the 1990s, hydraulic seals that acted as safety discharge valves were massively replaced by mechanical spring valves. Hydraulic seals represented simple and reliable devices ensuring protection levels 1 and 4 (25 and 100% of gas discharge, respectively). However, they required heating GDP rooms or using non-freezing liquids. Besides, the vent stack of a hydraulic seal, ensuring 100% capacity of a GDP, usually was not closed. This resulted in precipitation falling in the container, distorted physical height of device adjustment, and diluted non-freezing liquid.

However, it was 100% possibility of gas discharge that turned out to be difficult to ensure with spring devices. Technological capabilities of the industry (body casting, weight, size, etc.) significantly limited the capacity of safety discharge valves, and, according to the 2004 Polish industrial standard, devices with 100% capacity

were used only in GDPs with rated consumption of up to 60.0 m3/h and input pressure of more than 1.6 MPa.

In the rest of GDPs, spring safety discharge valves with the capacity of up to 25% of the rated consumption were used. Improved and safer pressure reduction lines also contributed to that. In such lines, besides the safety shut-off valve and safety discharge valve, there was also a regulator monitor. It was intended to adjust the operation of the main pressure regulator when it did not operate properly at high dynamics of input pressure. And in case of a failure of the main pressure reducer, the monitor took over its functions. Anyhow, the majority of GDPs became devoid of protection level 4 when the hydraulic seal actuated at 100% plant capacity at the pressure of 5 kPa.

It is difficult to comment on the experts' conclusion about the reduced diameter of the vent stack of the safety discharge valve. On the side of each valve, there is a hole with the internal thread for diameter corresponding to the rated capacity. The discharge pipe with such diameter is then led out above the GDP building. The height of the vent stack is calculated taking into account gas dispersion in such a way so that no explosive gas concentration formed in the lowest atmospheric layer. It is commonly at least 3.0 m above the ground level. It turned out impossible to establish if reduction to lesser diameter had been made. However, such reduction in diameter could not be critical to ensure gas discharge.

Data on the "siphonal", i.e. U-shaped layout of the discharge piping not protected against atmospheric precipitation, is far more important. For Polish GDPs, the piping should be L-shaped: it should be laid sideways through the wall, and then — directly upwards. We could try and explain why gas supply company employees implemented such seemingly illogical layout. No protection against moisture was commonly explained by a small diameter of the pipe. It was believed that no significant amount of precipitation could penetrate it. Nevertheless, some amount of water still penetrated the vent stack. Running down the pipe, it then entered the valve, resulting in corrosion. And in case water froze, the valve operation was completely interrupted.

Thus, the siphon could act as a condensate trap made at one's own risk, that protected the safety shut-off valve against moisture. It was assumed that when the valve actuated, water would just be driven off into the vent stack. Reduction in diameter of the discharge pipe might be caused by the use of the siphon made out of the material at hand. This is in fact a critical error made by the personnel: at a temperature below the freezing point, water in the siphon turns into an ice plug. In such case, when the safety discharge valve actuated, there was no way gas could be dumped into the atmosphere.

The situation is cleared up in the Zielona Góra city chronicle: "the first serious attack of winter" was recorded on 28.11.2010, i.e. two days before the accident. At 7 a.m., the thickness of the snow cover reached 37 cm, and the temperature was -11°C. This is where the chain of reasons related to the "human factor", which led to the accident in question, ends: long-term operation of the GDP with not

fully functioning equipment — disablement of the standby line safety shut-off valve — unlawful "siphon" layout of the discharge line — moisture entering the siphon — moisture freezing at a low temperature. The initiating factor of the accident was in fact a technical reason — a failure of the pressure regulator on the GDP standby line.

5. Analysis of technical and administrative measures

The prosecutor's investigation ends with determination of those guilty. For technical specialists, it is more important to determine a set of technical and administrative measures ensuring non-repetition of such accidents even at the worst combination of circumstances.

Just after the accident, operating teams of PGNiG (Polish oil and gas company) made a number of recommendations to subordinate regional offices that should have prevented such events. First, it was required to check the operation of all spring safety discharge valves. At GDPs where hydraulic seals were still installed, instrumental inspection of non-freezing liquids they were filled with was required.

Concurrently, a temporary solution was found to prevent accumulation of water in discharge lines (by means of small holes in the horizontal part of the vent stack). In case of rain, water could freely flow through such hole. It should be noted that this was in violation of the principle of preventing explosive gas concentrations from forming in the lower atmospheric layer. The hole was small, but in case of gas discharge, some gas was dumped into the atmosphere at a height of about 0.5 m above the ground level.

Figure 2. Standard termination of discharge and blowdown pipes at a Polish gas distribution unit plant

It was clear that it was just a half measure. That is why the next step was to structurally prevent moisture penetration in the vent stack. Hinged valves were quickly made at the end of the discharge pipe using materials at hand. The end of the pipe was often cut off at some angle. The valve opened under the pressure of the discharged gas, and after the discharge, it closed under gravity.

This should have made it possible not to make holes for water removal. However, such crude method had unavoidable consequences. Axes of the hinged joints became rusty, and sometimes they jammed, which made it difficult for the valve to open freely. And, which is

worse, a blow of wind could open the valve which further remained open.

Eventually, such devices started to be manufactured in a centralized way at factories (Figure 2). The use of proper materials increased valve reliability but did not rule out the possibility of precipitation penetration in the vent stack. Dirt, feathers, leaves, moisture freezing in a hinged joint — all this can degrade pressure integrity of a closed valve.

Any Russian specialist in gas supply would wonder why their Polish colleagues did not think of a simpler and safer solution. We are referring to the bend of the vent stack termination of about 180° downwards, traditionally used at our gas distribution plants (Figure 3). There are no moving parts that could "malfunction". Snow on the bend shown in the photo on the right demonstrates that there is no way for precipitation to penetrate the pipe.

Figure 3. Standard termination of discharge pipes at Russian low-pressure GDPs.

It is not that this way was not considered by the Polish gas supply industry. But the arguments for the solution with a hinged valve look strange. As follows from the explanations by Polish colleagues, they feared that gas outflow at a great speed during discharge could move the area of explosive gas concentration downwards, i.e. to the area of the GDP devices and the working repair crew. It was even assumed that gas flow could gradually wear out the pipe bend.

We will not go into those unreasonable concerns about the pipe "wear". Instead, we will consider a simple example. For a GDP with rated consumption of 60 m³/h with the 25% capacity of the discharge line, the gas outflow rate through the vent stack with a diameter of 25−30 mm would be 5−8 m/s. First, the gas jet that is 1.7 times lighter than air will bend upwards instantly. Besides, together with the rate increase, the ejecting capacity of the jet also increases, and it is diffused and slowed down by air. It is virtually impossible for an explosive gas concentration to form in the lower atmospheric layer at a gas outflow height of 4.5−5 m. Otherwise, this solution could not be used in Russian gas supply.

But it is not the only question. High gas outflow during gas discharge is quite rare. In case there are standard reasons behind the safety discharge valve actuation (low dynamics of the pressure regulator, contamination of the valve seat or damage to the membrane), the valve

operates in the pulse mode. Pressure in the discharge pipe increases gradually, the valve opens, and a small amount of gas is discharged into the atmosphere. Pressure drops drastically, the valve closes, and the pressure pulsation cycle repeats.

It shall be noted that actuation of the safety discharge valve shall be duplicated by a telemetric signal to the control unit of the gas supply company. In Western countries, in view of high dynamic characteristics of regulators, no discharge valves are usually stipulated in GDP layouts. There is only an alarm line transmitting a signal that gas pressure has increased to the set "alarm" level.

The Polish gas supply industry has developed in an in-between way. At large plants, where gas consumption and pressure variations are smoothed out, discharge devices are not installed. At GDPs subject to drastic variations in outlet pressure, safety discharge valves with the capacity of 2% of the plant rated consumption are provided. Such device is not regarded as an element of the safety system. It just "secures" the pressure regulator if the latter does not operate properly at high dynamics of pressure variations.

6. Origin of water in the system

It is seemingly a rhetorical issue. The prosecutor's investigation, without any hesitation, points at the atmospheric origin of the moisture accumulated in the "unlawful" siphon of the discharge pipe. This is based on an expert opinion that, however, was accepted a priori, without any observations or proof. In other words, it was based on the following assumption: "Where else it could possibly come from?"

Nevertheless, not rejecting such possibility, the authors would like to draw the reader's attention to another source of moisture in gas supply systems, i.e. the moisture of gas itself. According to standards of any country, dry gas should be supplied to city gas distribution systems. This stereotype has led to the fact that condensate traps that had previously been installed at the lower parts of connecting gas pipes and even under each riser, became gradually disused in design practice. Their use in gas distribution pipes became limited.

In fact, we are referring to the use of preliminarily dried gas that cannot be absolutely dry in principle. Otherwise, why would gas quality standards mention the dew point temperature for moisture (Federal Agency, 2014)? The authors dedicated a whole set of researches to the issues of gas fuel quality, including its humidity (Szkarowski, 2013, 2014). For purposes of this analysis, it is sufficient to provide an example that at the moisture content at the dew point level at the temperature of 0°C, the absolute humidity of gas is 4.88 g/m^3, which corresponds to 0.61% vol. This means that a gas distribution system that supplies 1 mln m^3 of gas, transports with it more than 6,000 m3 of moisture vapor.

The value of the dew point temperature in the certificates analyzed varied from +4 to −6°C. In reality, this figure can reach +20°C in operation. This means that during wintertime, gas is inevitably saturated with moisture vapor with its subsequent condensation.

Speculations about the origin of water in the system do not change the essence of the analysis: in this case, the accident would still happen due to a combination of unfavorable technical reasons and the human factor.

Conclusion

The analysis and the need for it can be easily criticized only on the basis that the situation described is unique and simply cannot happen again. However, we would like to point out that this accident should not and even could not have happened, if not for a chain of accumulated consequences making each other stronger, similar to the domino effect. We can even mention here the butterfly effect. Of course, an unlawfully disabled valve is not the same as a light beat of butterfly's wings, but the cause and effect mechanism is unrelenting. Our task was to draw the specialists' attention to the fact that there are no such aspects in gas supply that are less or more important. Every fault or erroneous action, despite their insignificance, can lead to tragic events.

The fact that the accident considered in this paper cannot be viewed as a unique one can be proved with a fresh example. On September 14, 2018, one man died and 12 more were injured after several dozen explosions related to gas leaks in three localities near Boston, USA (Interia Fakty, 2018). 50 fire teams participated in putting out fires in Lawrence, Andover and North Andover. Hundreds of people were evacuated. According to the preliminary firemen's conclusions, the reason behind the fires was too high gas pressure. No further comments are needed.

References

Ansari, N., Ayatollahi, S., Riazi, M. (2017). Underground natural gas storage in a low quality gas reservoir - Produced gas quality control by rate optimization. In: *Proceedings of 79th EAGE Conference and Exhibition 2017: Energy, Technology, Sustainability - Time to Open a New Chapter*.

Federal Agency on Technical Regulation and Metrology (2015). *GOST 5542-2014. Natural fuel gases for commercial and domestic use. Specifications.* Moscow: Standartinform.

Fu, X., Li, G., Zhang, X., Qiao, Z. (2018). Failure probability estimation of the gas supply using a data-driven model in an integrated energy system. *Applied Energy*, 232, pp. 704–714. DOI: 10.1016/j.apenergy.2018.09.097.

Interia Fakty (2018). *USA: series of gas explosions. Several dozen explosions*. Available at: https://fakty.interia.pl/swiat/news-usa-seria-wybuchow-gazu-kilkadziesiat-eksplozji,nId,2631139. (accessed on: 12.09.2018)

Kim, J.-H., Doh, D.-H., Choi, B.C. (2018). Evaluation of the ventilation safety requirements for the fuel gas supply system room of a gas-fueled vessel: Simulated leaks of methane and propane. *Journal of Mechanical Science and Technology*, 32 (11), pp. 5521–5532. DOI: 10.1007/s12206-018-1050-7.

Prokuratura Okrégowa (2013). *The indictment against the gas distribution network master in the case of gas explosion in Zielona Góra neighbourhood.* Available at: http://www.zielona-gora.po.gov.pl/index.php?id=3&ida=9326. (accessed on: 18.10.2018)

Super Express (2010). *Zielona Góra: Gas stove explosions in residential buildings.* Available at: http://www.se.pl/wiadomosci/polska/kuchenki-wybuchay-ludziom-w-domach_162460.html. (accessed on: 12.09.2018)

Szkarowski, A., Janta-Lipińska, S., Kolienko, A. (2013). Gas quality control as a tool of energy saving. *Gas, Water and Sanitary Engineering*, 4, pp. 146–150.

Szkarowski, A. (2014). *Gas combustion. Theory, practice, ecology.* (Warsaw: WNT Publishing House).

Tymchik, G.S. et al., (2018). Quality control system of well-bonded coupling fitting onto high pressure gas-main pipelines. In: *Proceedings of SPIE - The International Society for Optical Engineering*, 108085A. DOI: 10.1117/12.2501594.

Vasista, T.G., Alsudairi, M.A.T. (2018). Managing through computer aided quality control in oil & natural gas industry project sites. *Journal of Advanced Research in Dynamical and Control Systems,* 10 (4), pp. 896–905.

Wang, Y., Yang, S. (2018). Proposal and thermodynamic analysis of a combined open-cycle absorption heat pump and thermal desalination system driven by high-humidity exhaust gas. *Desalination*, 448, pp. 93–102. DOI: 10.1016/j.desal.2018.10.003.